



INTERPRETATION OF GEOPHYSICAL WELL LOGS FROM THE NESJAVELLIR GEOTHERMAL FIELD, ICELAND

Arturo Quezada Muñoz

Comisión Ejecutiva Hidroeléctrica del Río Lempa (C.E.L.),
Gerencia de Recursos Geotérmicos,
km 11 ½ Carretera al Puerto La Libertad,
Santa Tecla,
EL SALVADOR

ABSTRACT

Porosity and SiO₂ content as a function of depth has been calculated using the data of caliper, natural gamma and neutron-neutron logs of twelve wells from the Nesjavellir geothermal field, SW-Iceland. The obtained values have been interpreted and compared with other available geological data. A unimodal distribution of the porosity, with a maximum of 19%, and a good correlation between relatively high porosity zones and hyaloclastite layer locations have been found. It seems that the major feedzones in the wells found during drilling are located in relatively high porosity zones. The SiO₂ content distribution is also unimodal, with a maximum of 44.5%. Even though the SiO₂ logs show several peaks which can be associated with intermediate and acidic magmatic intrusions, there is not a clear correlation between the wells. In the lower part of the rock sequence the mean porosity in the central part of the well field is higher than in the outer parts. The porosity contour maps are elongated from southwest to northeast, associated with the fracture trend in the field. This result is similar to the behaviour shown by other parameters of the field such as pressure and temperature. A very good correlation in the porosity categories has been found for the depth interval 600-1000 m b.s.l. between the results of the porosity logs and the porosity categories used in the modelling of this geothermal field in 1992. Even though there is a discrepancy in the porosity categories between wells NG-10 and NJ-11, there is also, in general, a good correlation in the results for the depth interval 1000-1800 m b.s.l.

1. INTRODUCTION

The Nesjavellir high-temperature geothermal field is located in the northern part of the Hengill geothermal area, and is one of the largest in Iceland. It is within a SW-NE trending fissure swarm in the volcanic rift zone, in SW- Iceland (Figure 1). Geophysical logs like natural gamma ray logs, neutron-neutron logs, resistivity logs and caliper logs have been carried out in all the wells during their drilling and after they were completed. The main objectives of the present report are to review the natural

gamma ray and neutron-neutron logs carried out in the wells (NG-6, NG-7, NG-9, NG-10, NJ-11, NJ-12, NJ-13, NJ-14, NJ-15, NJ-16, NJ-17 and NJ-18) and to do a comparison with the geological data in order to figure out some correlations.

This project report is the final part of a six months training course, from April to October 1996, for the Fellows of the United Nations University Geothermal Training Programme at Orkustofnun, National Energy Authority of Iceland.

2. THE NESJAVELLIR GEOTHERMAL FIELD

Nesjavellir geothermal field is located in the northern sector of the Hengill central volcano, within a SW-NE trending fracture zone which intersects the volcano. In the uppermost part (above 400 m b.s.l.) basaltic hyaloclastite formations dominate the rock sequence, while the lower part is characterized by basaltic lava series, with sparse hyaloclastite formations interbedded. Magmatic intrusions become more frequent with depth, compose less than 5% of the rock sequence above 400 m b.s.l., around 20% between 400 m b.s.l. and 1300 m b.s.l., and more than 50% at 1300-1600 m b.s.l. The majority of these intrusive rocks are of basaltic composition with apparent thicknesses of less than 30 m. Below 1400 m b.s.l. intermediate composition intrusive rocks have been found.

An intrusion of acid composition is encountered below 2100 m depth in well NJ-11 (Franzson et al., 1986). The basaltic hyaloclastites and the basaltic lavas have a similar silica (SiO_2) content, with typical values between 46-50%. The silica contents of the intrusions are: basaltic composition, 46-52%, intermediate composition, 52-56% and diorite, 62% or more. These values have been obtained from fresh samples. On the other hand, qualitatively, the primary porosity of the hyaloclastites is higher than the basaltic lavas (Franzson, 1996, pers. comm.). In the bottom of well NJ-11 (2265 m deep) a temperature higher than 380°C has been measured, which is the highest temperature measured in a geothermal well in Iceland and an aquifer pressure in excess of 220 bar is suggested. The high temperature and pressure indicate supercritical fluid conditions in the deep aquifer of the Nesjavellir system (Steingrímsson et al., 1990).

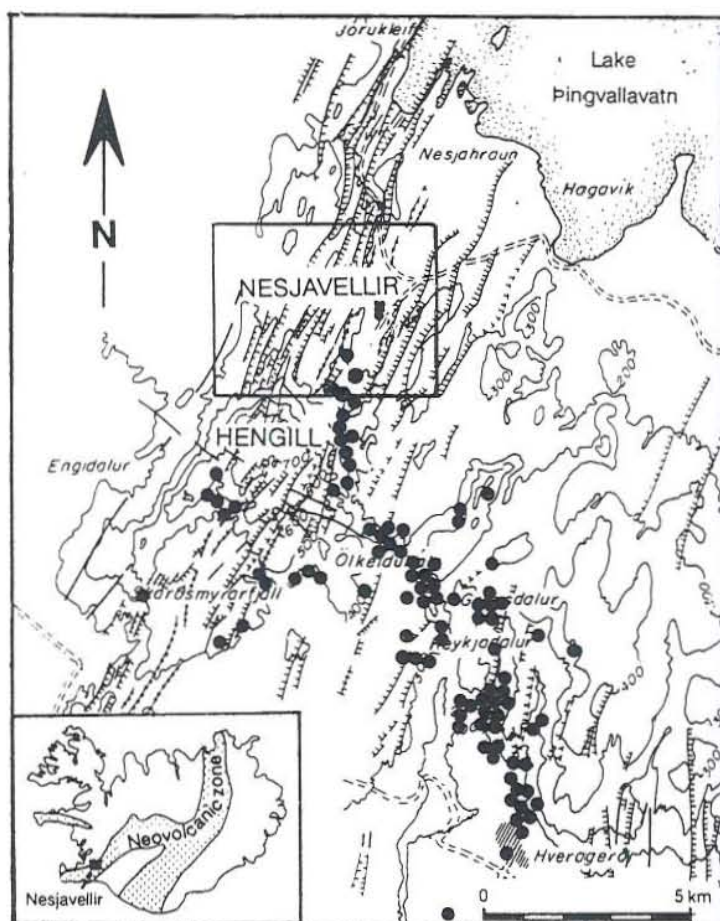


FIGURE 1: Tectonic map of the Hengill area, the location of active geothermal manifestations (hot springs and fumaroles) is shown with black dots; the Nesjavellir field is situated within the square (Gunnarsson et al., 1992)

Eighteen wells were drilled during the period from 1965 to 1986. The first five wells (1-5), drilled between 1965 and 1972, identify the presence of a high-temperature reservoir. The other

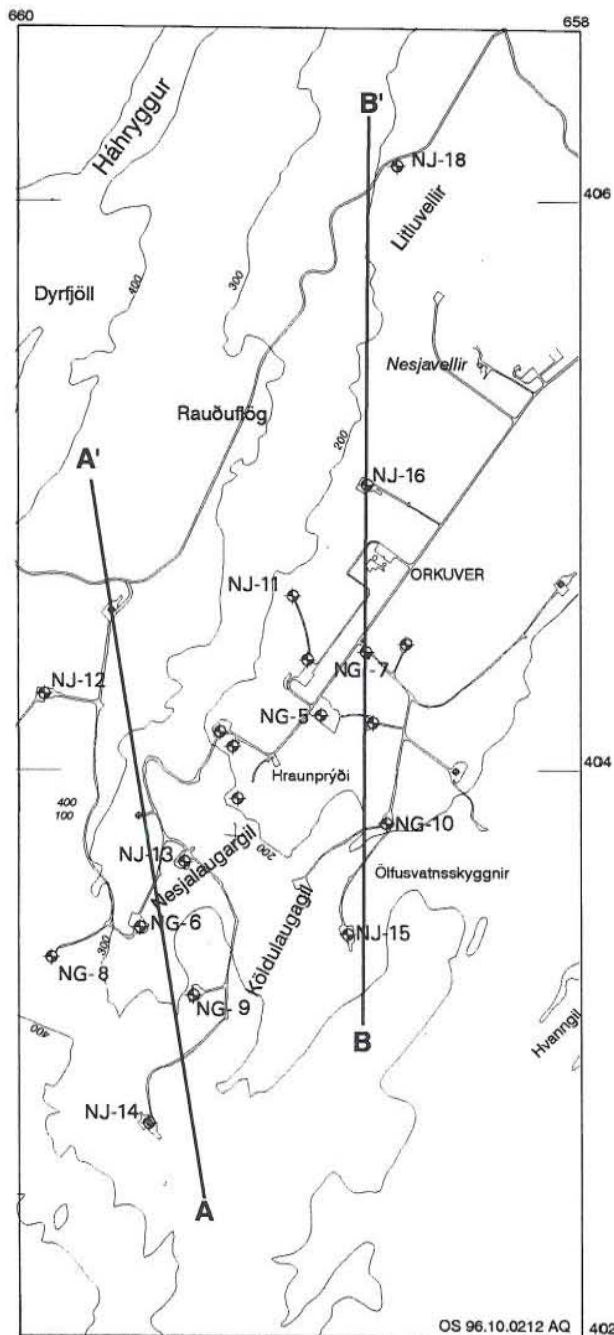


FIGURE 2: The Nesjavellir well field and location of the geological cross-sections

thirteen wells (6-18) were drilled between 1980 and 1986. All of these wells are potential producers with the exception of well NG-8, which is 400 m deep (Franzson and Sigvaldason, 1985). Figure 2 shows the location of the wells and the geological cross-sections that have been related to the geophysical logs. The well field covers a land area of 3.5 km². All the wells penetrate the geothermal reservoir and the total thermal power produced by them is 754 MW_t (Gunnarsson et al., 1992). A building has been designed in several phases, for a co-generation power plant with a planned full capacity of 400 MW_t for district heating and over 80 MW_e for electricity production (Gunnarsson et al., 1992). At present the production is 300 MW_t for the Reykjavík Municipal District Heating Service.

Böðvarsson et al. (1990) hypothesized that the main upflow zone of the system is under the Hengill volcano. They estimated that the permeability and porosity of the system are very heterogeneous with an average permeability of 5 mD and an "effective" porosity of 5%, in the upper part of the reservoir, whereas 10 mD and 3.5% have been estimated in the lower part.

3. GEOPHYSICAL LOGS

The well-logs or wireline logs are obtained by means of measuring equipment (logging tools or downhole sonde) lowered on cables (wireline or transmission line) into the well. The log signal is transmitted up the cable (which contains one or several conductors) to a surface registration unit. The recording of this information on film, magnetic tape, computer memory or paper constitutes the well-log. Well logging is performed after an interruption or the termination of drilling activity (Serra, 1984).

3.1 Geothermal logging methods

The logging methods and measurements described below are the most frequently used today in geothermal investigation.

3.1.1 Temperature log

The temperature is the fundamental parameter in geothermal investigation. At present the temperature sensors most frequently used in well logging are resistance thermometers and mechanical thermometers. The temperature log, as well as the pressure, fluid density and flow metre logs, is called the production log and can be performed either in open or cased holes.

The resistance temperature sensors most commonly used are platinum sensors, which have a near linear temperature-resistance relationship, and thermistors, which have a non-linear temperature-resistance relationship; as the temperature increases the resistance of thermistors decrease. The operation temperature of resistance thermometers is limited, but special electrical insulators of teflon are available for temperatures up to 260°C. However, the maximum operating temperature of commercial high temperature semi-conductors is still below 200°C. These thermometers have the advantage of small size and ease of transmission of the signal through an electrical cable, from the measurement point to a surface recorder, but need downhole electronics. They need to be calibrated regularly, due to the drift of their electrical properties with time.

The mechanical thermometers are used mainly in high temperature wells. The temperature data is recorded inside the probe on a clock-driven recorder. They can be operated up to 350°C. The temperature sensors used are the bourdon tube (Amerada gauge), in which the boiling pressure of a special fluid is recorded, and bimetal (Kuster gauge), which uses the expansion of the bimetal to indicate the temperature. These two types of sensors also need to be calibrated regularly, due to their drift with time. The accuracy of the commercial mechanical thermometers is no better than $\pm 1^\circ\text{C}$.

3.1.2 Pressure log

In low-temperature wells the pressure of the geothermal system, at least at the well site, is nearly correctly determined by measurement of the water level of the well or the wellhead pressure if the well is artesian. In high-temperature wells pressure logging is widely used. The pressure at any point of the well is measured using mechanical pressure gauges, which are quite similar to the bourdon tube thermometers. The pressure gauge of the bourdon tube is open to the well fluid, and is therefore sensitive to the pressure at the measurement point of the well. The pressure is recorded inside the probe on a clock-driven recorder which also needs to be calibrated regularly. The accuracy of the commercial pressure gauges is ± 0.1 to 1 bar.

3.1.3 Caliper log

The measurement of the diameter of a well is made by using a caliper tool. There are several types of sondes. The ordinary type has three arms, but tools with up to 60 arms are available. The arms are linked to the cursor of an electrical potential metre. Variations in the borehole diameter are reflected in resistance changes shown in the potential metre. Calibration allows comparison of resistance changes to diameter changes. An electrical motor inside the caliper tool opens or closes the arms. Due to the electrical cable and the downhole electronics, high temperature wells must be quenched with cold water before the logging can be carried out. The maximum operating temperature of this tool is 150-200°C.

The caliper logs are of great importance in well log analysis, where they allow the correction of several types of logs for the the borehole in order to get a more precise interpretation. The caliper logs are also used for:

- a) The detection of porous and permeable zones (mud cake presence) and the determination of the mud cake thickness;
- b) The measurement of hole volume in order to obtain an estimation of the cement volume needed;
- c) Detection of consolidation and in gauge sections for the scaling of packers for well testing;
- d) Location of cavities in wells and casing damages;
- e) Locating depositions (calcite scaling) in wells;
- f) A guide to lithology.

3.1.4 Natural gamma ray log

The natural gamma ray log measures the natural radioactivity of rock formation due to the presence of radioactive isotopes and is used in geothermal investigations to estimate bed boundaries and determine lithology. Therefore, natural gamma ray logs are performed in order to measure the electromagnetic radiations or photons that are emitted by a nucleus in an excited state.

The isotopes that are mainly responsible for radiation are potassium (^{40}K isotope) and those involved in the decay series of uranium (^{238}U) and thorium (^{232}Th). There are three types of radiation emitted in the spontaneous disintegration of these radioisotopes, the alpha particles, beta particles and gamma rays. Due to the short penetration length of alpha and beta particles it is the gamma radiation that is detected. The detectors used are both the Geiger-Müller counter (ionization chamber containing inert argon gas under low pressure) and the scintillation counter (sodium iodide crystal doped with thallium). The Geiger-Müller counter measures the total gamma intensity, and the scintillation counter can register the energy spectrum of the gamma radiation. The scintillation detector is used most since it is more efficient and the short length allows good formation definition. The count rate measured by a gamma ray tool at each depth in a borehole is related to the concentration of the radioisotopes in the formation. This quantity is called the radioactivity of that formation. Gamma ray logs are recorded in API (American Petroleum Institute) gamma ray units. The API gamma ray unit is defined as 0.5% of the difference in count rate registered between zones of low and high radioactivity in a test pit situated at the University of Houston, Texas, U.S.A. (Figure 3). The gamma ray tools can be used in either cased or open holes, above and below the water level. The maximum operation temperature of these standard tools is 150-200°C, but some companies have developed special equipment, with maximum operating temperatures of up to 260°C (Chambre Syndicale de la Recherche et de la Production du Pétrole et du Gaz Naturel, 1984).

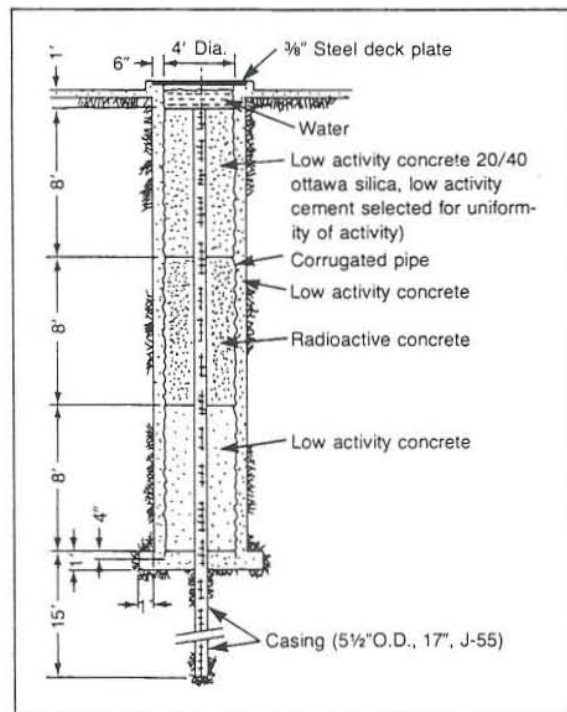


FIGURE 3: The American Petroleum Institute (API) gamma ray calibration pit located at the University of Texas, Houston (Helander, 1983)

In common igneous rocks, ^{40}K and ^{238}U contribute about equally to the total count rate and the typical contribution of ^{232}Th is as much radiation as ^{40}K and ^{238}U combined. In acidic rocks the concentrations

of all three elements are around ten times greater than in ultrabasic rocks. Also the concentration of these elements are greater in acidic rocks than in intermediate and basic rocks (Figure 4). The concentrations are, in general, proportional to the SiO_2 content (Hearst and Nelson, 1985).

In Icelandic volcanic rocks the response of the gamma ray log have been investigated. A strong correlation between the SiO_2 and the concentration of ^{232}Th , ^{238}U and ^{40}K has been found. A linear relationship has been established between the SiO_2 content of volcanic rocks and natural gamma ray intensity.

The gamma ray log is found to be a very good method to identify acid layers in the strata. The silica rich layers occur sporadically in the basaltic pile of Iceland and should hence be good trace layers for correlation between wells (Stefánsson et al., 1982). In a geological environment where the rock is mainly basaltic, the natural gamma ray log will generally show low intensity with a few peaks due to more acid units located between the basic rocks. On the other hand, in regions where the rocks are generally acid (back arc volcanic regions), a gamma ray intensity, generally high with few minima due to more basic units in the formation strata, is expected (Stefánsson and Steingrímsson, 1980).

3.1.5 Neutron-neutron log

Neutron-neutron logs provide an estimate of the formation porosity. The neutron-neutron logs are measurements of the apparent concentration of hydrogen atoms per unit volume in the formation and, therefore, in clean formations reflect the liquid filled porosity. In the neutron-neutron tool a neutron source (Americium-Beryllium or Radium-Beryllium) bombards the formation with energetic neutrons, emitted at high speed and energy. During their travel through the borehole and formation they will experience numerous collisions with the nuclei present. If these nuclei are hydrogen, the neutrons are slowed down rapidly until thermal state is reached, and they can be captured. This capture is accompanied by emission of gamma radiation. As the hydrogen content of the material surrounding the source increases, the neutrons will be captured sooner and, therefore, fewer fast or slow neutrons will reach the detector, resulting in lower count rates. In the thermal state the thermal energy of a neutron is 0.025 eV which represents the final stage of the slowing down phase of the neutrons. The term epithermal is applied to the energy range 100 eV - 0.1 eV. The detector used in the neutron logs can be

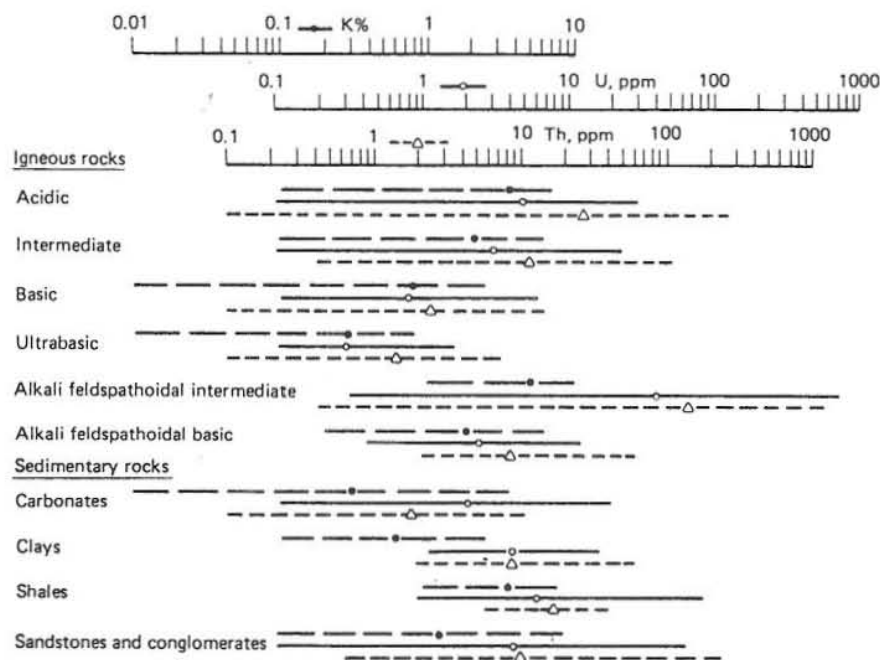


FIGURE 4: Range of mean values of K, U and Th in igneous and sedimentary rocks; scales have been shifted so that all three elements produce comparable count rates in a NaI detector; for example, 1 ppm U produces the same count rate as 0.95% K and 2.13 ppm Th; left edges of some lines extend to concentrations less than given by scale (Hearst and Nelson, 1985)

either a slow neutron detector (^3He) for the detection of thermal neutrons or a gamma detector (Geiger-Müller counter). At present, there are also neutron-neutron tools which use an epithermal neutron detector (activated boron fluoride or lithium fluoride crystals). The neutron-gamma tool and the neutron-thermal neutron tool can be performed in either cased or open holes; however, the presence of casing tends to decrease the counting rate and porosity resolution, because the casing absorbs both neutron and gamma rays. The neutron-epithermal neutron tool can be used only in open holes, empty or liquid-filled. The maximum operating temperature of these standard tools is 150-200°C, however some companies

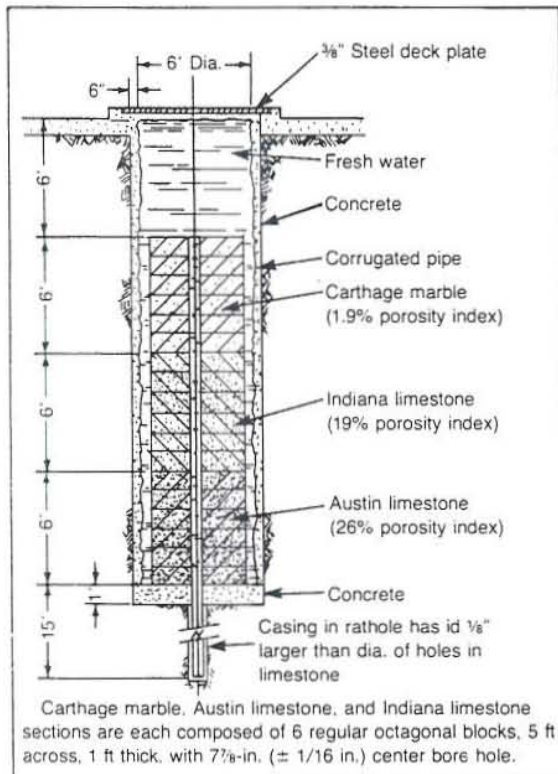


FIGURE 5: The American Petroleum Institute neutron calibration pit situated at the University of Texas, Houston. (From Helander, 1983)

have developed special equipment, with maximum operating temperatures of up to 260°C (Chambre Syndicale de la Recherche et de la Production du Pétrole et du Gaz Naturel, 1984).

Neutron-neutron logs are recorded in API neutron units. The API neutron unit is defined as a 1/1000 of the deflection from zero recorded when a tool is located opposite the Indiana limestone section of the neutron calibrated pit at the University of Houston (Figure 5).

3.1.6 Gamma-gamma log

The gamma-gamma log or density log is primarily used to evaluate the formation porosity; however, it is intensively used in conjunction with neutron and resistivity logs to identify lithology. In this type of tool a gamma ray source (^{60}Co or ^{137}Cs) emits gamma rays (photons) into the formation. These gamma rays interact with the electrons in the material opposite the source. The predominant interaction is Compton scattering, where each time the gamma ray strikes an electron it changes direction and loses some energy. The density tools measure by means of a scintillation detector the intensity of scattered gamma rays at a fixed distance from the source. This intensity is a function of the

electron density of the formation. The electron density is proportional to the bulk density of the formation. As the bulk density of the formation increases, the probability of more collisions, between the gamma ray and the electrons in a fixed distance increases, leading to a greater loss of energy, and also absorption of some gamma rays (photo-electric effect).

The density log tool is calibrated in three steps, an initial laboratory calibration is made in pure limestone saturated with fresh water. Secondary calibration is made in blocks of aluminium and sulphur or magnesium. Finally, a calibration jig is used at the wellsite. After the introduction of two detector tools, the surface instrumentation transforms the measurement units and the log is given directly in grams per cubic centimetre (g/cm^3). At present the maximum operating temperature of these tools is 200-250°C.

3.1.7 Resistivity log

In order to determine true formation resistivity, several resistivity measuring tools have been developed, due to the great variety of borehole and formation characteristics. There is still no single resistivity

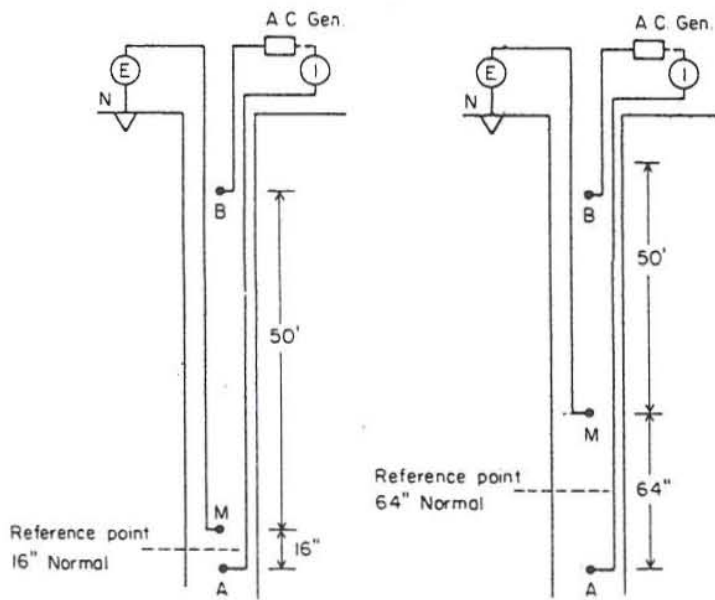


FIGURE 6: Electrode array for the short (16") and long (64") normal resistivity log configurations (Keys and McCary, 1971; Stefánsson and Steingrímsson, 1980)

N electrodes is $V = V_M - V_N = V_M$. Assuming an infinite homogeneous medium, the apparent resistivity (ρ) of the formation is given by the formula:

$$\rho = 4\pi \times AM \times \frac{V}{I} \tag{1}$$

The normal resistivity configuration shows the apparent resistivity variations of the medium surrounding the sonde. The determination of the true resistivity of the formation will, therefore, include elimination of well effects (well size and fluid resistivity) as well as the effects of limited bed thickness of the adjacent lithological units and their resistivity relative to the resistivity of the formation of interest. Normal resistivity logs can be performed only in the uncased part of the well below water level. Standard tools with maximum temperature and pressure operating conditions of 177°C and 20 000 psi are available.

Numerous additional logs are utilized in geothermal investigations. In Table 1 a summary is given of logging methods and parameters which are measured or can be measured in geothermal wells (Stefánsson and Steingrímsson, 1980).

3.2 Available data

The basic data that have been used to carry out the present research are the sets of caliper, natural gamma and neutron-neutron logs performed during or after the drilling of the wells at Nesjavellir from October 1982 to October 1986. Detailed information about log number, well identification, type of log, date, starting depth and final depth is given in Table 2. In Appendix I these logs are shown graphically.

logging tool applicable to all situations. Here, only the normal resistivity log will be briefly described.

The normal resistivity log is a four electrodes configuration, one electrode is at the surface and three electrodes are in the hole. Two of these three are fixed on the sonde and the other one is usually the armour of the logging cable. There are two conventional AM spacings for the normal resistivity log, as shown in Figure 6, $AM = 16$ inches (short normal) and $AM = 64$ inches (long normal). A generator drives a constant current I from A to B . The potential V_M of M is measured with respect to a reference N (at zero potential) by means of a voltmeter. If $V_N = 0$, the voltage between M and

TABLE 1: Logging parameters that can be measured in geothermal wells
(Stefánsson and Steingrímsson, 1980)

Type of log	Parameter measured	Type of detector	Information obtained
Temperature log	Temperature	Resistor, bourdon tube or bimetal	Reservoir temperature, location of aquifers, temperature gradient, heat flow
Differential temperature log	Temperature difference between two locat. in well	Resistor and delay	Location of aquifers
Pressure log	Pressure	Crystal or bourdon tube	Pressure in reservoir. Time dependent pressure gives information on permeability. In some cases flow direction. Response of field to utilization
Caliper log	Hole diameter	Movable arms	Location of cavities in well, casing damages
Natural gamma ray log	Total gamma radioactivity of rock	Geiger-Müller counter or scintillation counter	Differentiation of rock, sensitive to hole diameter
Gamma-gamma log	Scattered and attenuated gamma radiation	Geiger-Müller counter or scintillation counter	Bulk density of surrounding rock, sensitive to hole diameter
Neutron-neutron log	Neutron slowed down and scattered by hydrogen	³ He neutron detector	Porosity of surrounding rock, sensitive to hole diameter
Spontaneous potential log	Natural electrical potentials	Electrode	Probable streaming potential in well
Resistivity log	Resistivity of hole and adjacent rock	Electrode	Porosity of rock. Salinity and temperature of fluid
Sonic velocity log	Vertical component of compressional sonic wave	Hydrophone	Porosity of rock. Rock type
Casing collar locator (CCL) log	Differential magnetic permeability adjacent to sonde	Permanent magnet and two coils	Location of casing joints. In some cases casing damage can be localized
Sonic bond log	Attenuation of sonic wave	Hydrophone	Quality of cement outside casing. In an open hole it can give density of fractures in the well
Directional survey	Dip and direction of well	Pendulum and compass	Three dimensional location of the well
Flow metre log	Fluid velocity in well	Spinner	Flow and flow direction in well. Location of aquifers
Fluid sampler	Sample of fluid	Bottle	Composition of fluid at various depths
Side wall core gun	Sample of rock	Piston cylinder	Composition of rock at various depths
Borehole televiewer	Reflective acoustic wave from wells of the hole	Sonic detector	Fractures in the borehole walls
Magnetometer log	Vertical or total magnetic field	Fluxgate or nuclear magn.resonance (NMR)	Magnetic polarity of geological units transversed
Free point log	Differential extension of torsion of the drill-string	Extension metre or torsion metre	Highest free point of the drill-sting

3.3 Depth reference

The method used to get the depth correction is to cross-correlate the caliper and the neutron-neutron logs, which have different offsets at depth. The zero shift is determined by finding a minimum in the cross correlation using the BHMCOV program (Arason, 1993). Neutron-neutron and natural gamma ray logs are measured by the same probe, giving a fixed depth offset of 1.6 m between them. After calculation of the offset value between the caliper log and the neutron-neutron log, this value was used to correct the depth values in the caliper log. This was done for all the wells analysed. The offset values that have been found for these logs vary in range from -2.3 m to 1.5 m, with an average value of 0.05 m.

3.4 Caliper correction

As the natural gamma radiation and the neutron count rates are, as other log parameters, sensitive to the well diameter, caliper correction is done to the logs. This correction is carried out for each well with computer programs that calculate porosity and SiO₂ content.

TABLE 2: General information about the caliper (C), natural gamma (G) and neutron-neutron (N) logs from Nesjavellir geothermal field, used as basic data

Well No.	Log number	Log type	Date	Start depth (m)	Final depth (m)
NG-6 (95006)	5104	N	16-10-82	1.4	604.0
	5107	C	16-10-82	198.8	626.8
	11433	G	16-10-82	0.6	602.0
	3568	N	29-10-82	619.6	1102.6
	3570	C	29-10-82	394.8	1103.8
	11432	G	29-10-82	610.4	1100.6
NG-7 (95007)	924	C	30-10-83	10.5	575.7
	926	N	30-10-83	83.3	575.7
	930	C	13-11-83	500.1	1688.9
	932	N	13-11-83	500.3	1689.1
	10839	G	13-11-83	605.8	1989.0
NG-9 (95009)	956	N	21-09-84	169.4	1042.2
	957	C	21-09-84	742.7	1032.3
NG-10 (95010)	963	N	03-10-84	38.3	189.1
	966	C	03-10-84	37.9	189.1
	11518	G	03-10-84	38.3	184.3
	972	N	15-10-84	200.7	598.3
	974	C	15-10-84	192.7	584.7
	11523	G	15-10-84	197.1	593.9
	967	N	04-11-84	600.0	1777.2
	968	C	04-11-84	591.9	1777.1
	11522	G	04-11-84	599.1	1777.5
NG-11 (95011)	997	C	28-05-85	12.7	1412.3
	998	N	28-05-85	564.6	1420.2
	11528	G	28-05-85	549.2	1402.8
NG-12 (95012)	1006	C	18-06-85	9.0	269.5
	1007	N	18-06-85	2.8	266.8
	11531	G	18-06-85	20.0	266.0
	1014	N	26-06-85	274.3	754.2
	1011	C	26-06-85	377.5	766.5
	1026	N	14-07-85	752.0	1799.5
	1027	C	14-07-85	749.0	1800.0
	11529	G	14-07-85	751.5	1800.0
NG-13 (95013)	1032	C	24-07-85	0.5	277.5
	1035	N	24-07-85	4.4	277.2
	11534	G	24-07-85	9.6	276.4
	1041	C	31-07-85	243.0	813.5
	1038	N	31-07-85	231.1	599.7
	11533	G	31-07-85	231.1	599.7
	4748	N	20-08-85	651.5	1580.7
	4749	C	20-08-85	800.5	1580.0
	11532	G	20-08-85	651.5	1580.7

Well No.	Log number	Log type	Date	Start depth (m)	Final depth (m)
NJ-14 (95014)	4623	N	31-08-85	24.1	296.1
	4626	C	31-08-85	18.7	290.3
	11537	G	31-08-85	22.5	294.5
	4615	N	05-09-85	189.6	780.0
	4617	C	05-09-85	282.8	765.6
	11536	G	05-09-85	188.0	778.4
	4597	N	13-09-85	700.6	1209.8
	4598	C	13-09-85	716.5	1202.0
	11535	G	13-09-85	693.9	1208.3
NJ-15 (95015)	4691	N	26-09-85	31.6	271.6
	4693	C	26-09-85	9.2	268.4
	11540	G	26-09-85	43.1	273.5
	4673	N	06-10-85	230.7	782.3
	4674	C	06-10-85	202.7	782.7
	4657	N	19-10-85	744.0	1648.8
	4659	C	19-10-85	750.0	1668.8
	11538	G	19-10-85	743.9	1647.5
NJ-16 (95016)	4788	N	01-11-85	22.3	269.1
	4789	C	01-11-85	54.7	267.1
	11543	G	01-11-85	23.5	270.7
	4773	N	09-11-85	211.8	796.2
	11542	G	09-11-85	221.8	559.0
	4771	C	10-11-85	250.2	776.6
	4830	N	24-11-85	773.5	2025.5
	4832	C	24-11-85	101.9	2013.9
NJ-17 (95017)	1052	N	26-06-86	263.6	770.0
	1053	C	26-06-86	263.6	765.2
	11544	G	26-06-86	263.6	769.6
	1056	N	23-08-86	770.4	1869.2
	1057	C	23-08-86	770.0	1865.6
	11561	G	23-08-86	770.0	1870.8
NJ-18 (95018)	1064	C	23-09-86	259.2	940.9
	4715	N	23-09-86	206.8	938.4
	4723	C	13-10-86	965.5	2008.0
	4726	N	13-10-86	897.6	2002.0
	11545	G	13-10-86	901.6	1905.2

4. INTERPRETATION OF DATA

4.1 Porosity

Formation porosity is estimated from the neutron-neutron logs, using the caliper logs values as a correction factor. The BHMPOR program (Arason, 1993) was used to determine the porosity in all the wells. Calculated porosity values as a function of depth for all the analysed wells are shown in Figure 7. Figure 8 shows the porosity distribution for all the wells analysed here. The distribution is unimodal with a maximum peak at 19% porosity. Distribution histograms have been made for each well and most of the wells have unimodal distribution with peaks around 19%, with the exception of wells NJ-16 and

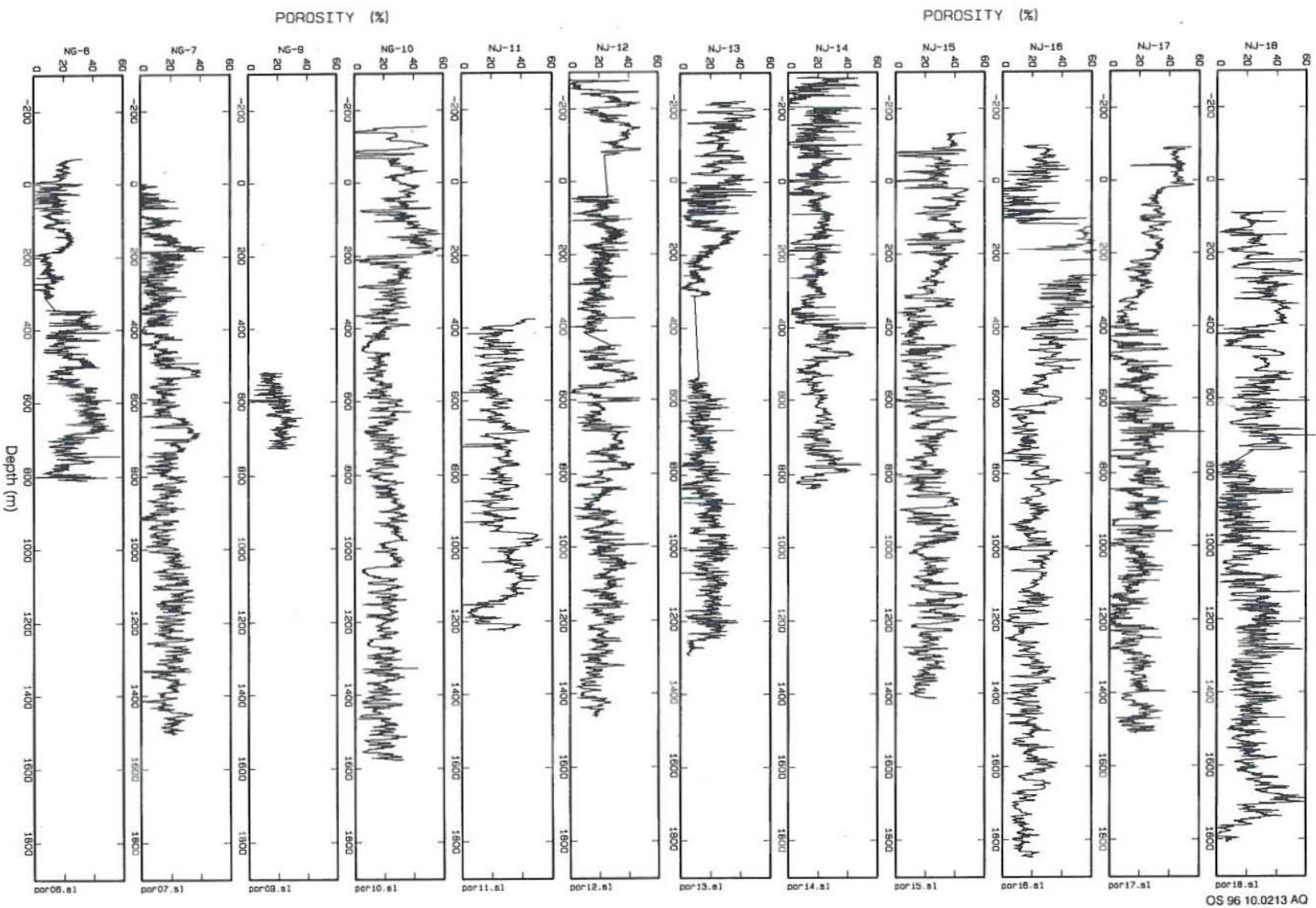


FIGURE 7: Calculated porosity as a function of depth for all the analysed Nesjavellir wells

NJ-16 and NJ-17 (See Appendix II).

They have bimodal distribution, with a peak around 21% and a smaller one at 45-50%. The porosity data was divided into two parts, above 800 m b.s.l. and below. Figure 9 shows histograms of these groups. The results show in both cases a maximum peak around 20% porosity. However, the histogram of the data below 800 m b.s.l. is sharper than that above. This means that there is less variation in the porosity values below 800 m b.s.l., where the basaltic lavas are predominant and the magmatic intrusions become more frequent. Something similar occurs with the relationship between the number of the main feedzones detected during the drilling of the wells and the porosity, as shown in Figure 10. It also shows that most of the main feedzones are associated with values of 15-20%.

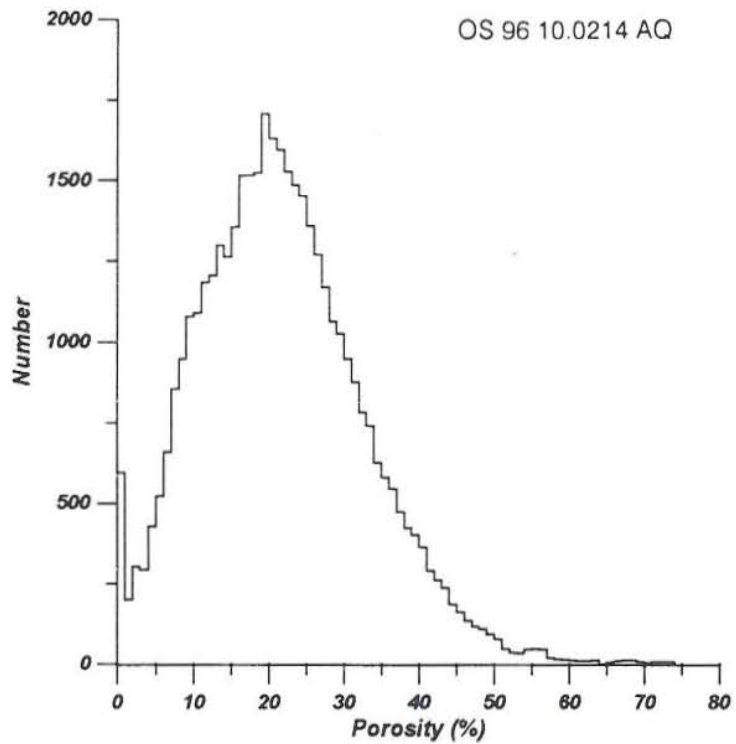


FIGURE 8: Porosity distribution, using all the well data

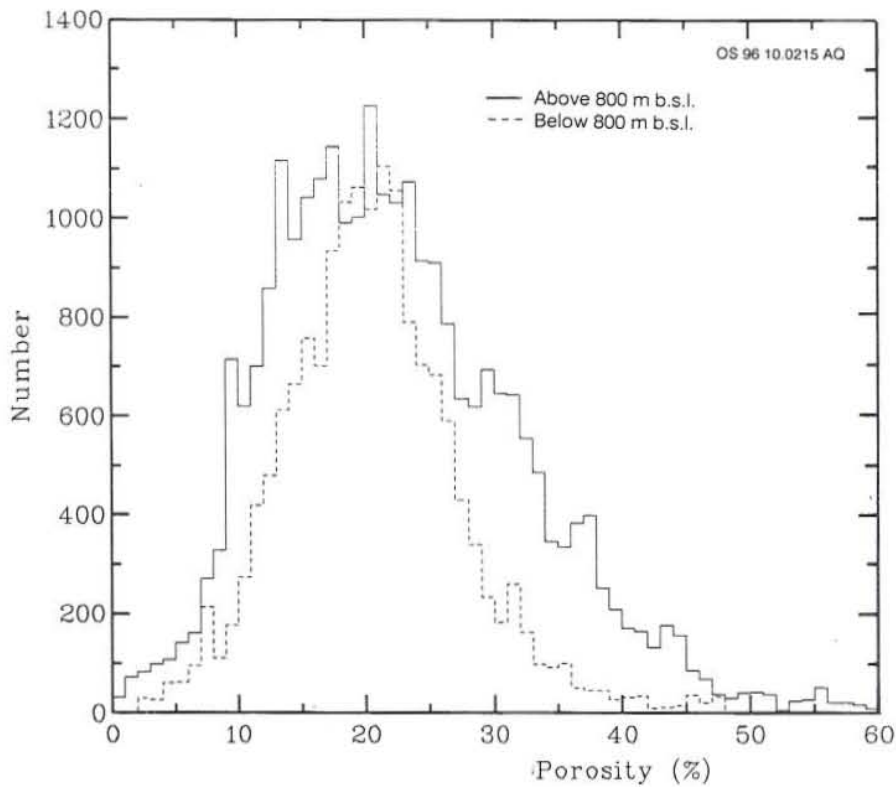


FIGURE 9: Porosity distribution above and below 800 m b.s.l. for the Nesjavellir wells

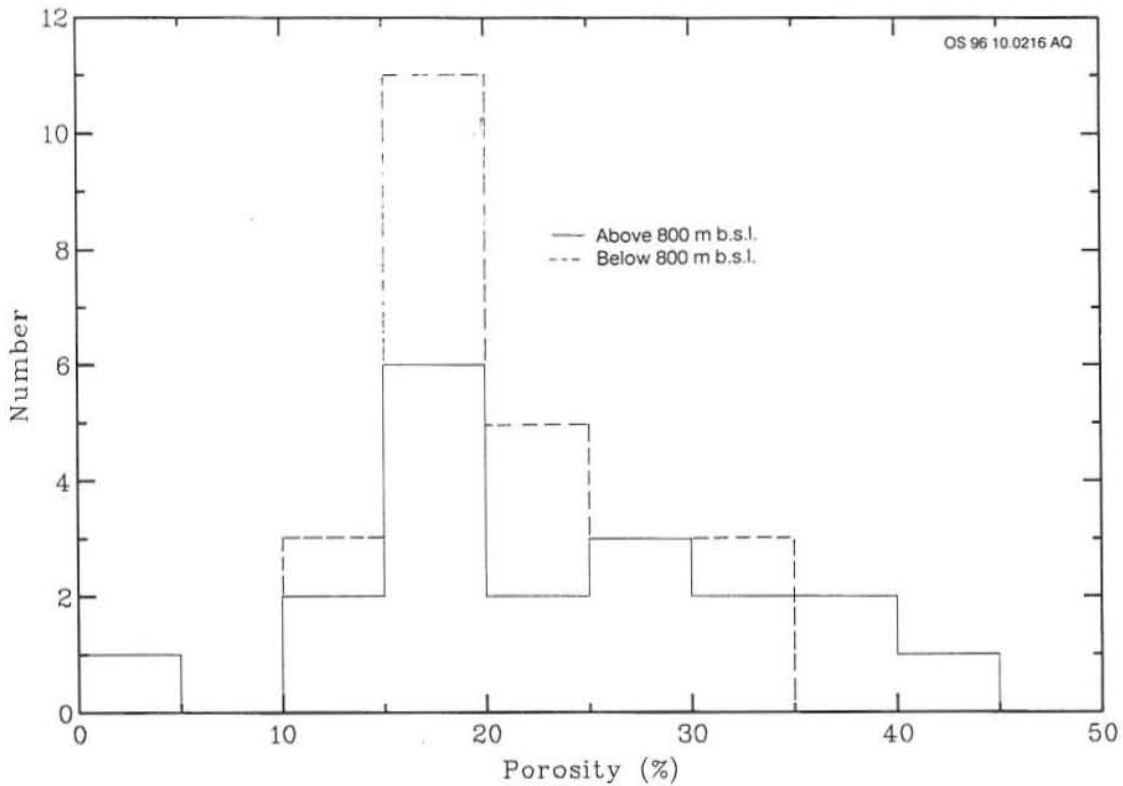


FIGURE 10: Distribution of main feedzones vs. porosity, above and below 800 m b.s.l.

4.2 SiO₂ content

In order to determine the percentage of SiO₂ content in a formation, the following equation was used:

$$SiO_2(\%) = 40.6 + (0.264 \times I_o \times C) \tag{2}$$

where

I_o = Intensity of gamma radiation, in API units;

C = Caliper correction factor, which is calculated using the following equation:

$$C = \frac{1}{1.192 - 0.3937 \log \left[\frac{cal.(mm)}{20} \right]} + \frac{0.32}{\left[\frac{cal.(mm)}{20} \right]^2} \tag{3}$$

where

$cal.(mm)$ = Diameter of the well, in mm, at corresponding depth, measured by the caliper log.

The BHMSIO2 program, based on the equations above (Arason, pers. comm.), has been used to determine the SiO₂ content of the formation for all the wells. Calculated values of silica content as a function of depth for all the wells analysed are shown in Figure 11. Even though the SiO₂ logs show several peaks which can be associated with intermediate and acidic magmatic intrusions, there is not a clear correlation between wells. Figure 12, which has been made using the SiO₂ data of wells NG-6, NG-7, NJ-11, NJ-12, NJ-13, NJ-14, NJ-15, NJ-16, NJ-17 and NJ-18, shows a unimodal distribution of SiO₂ content, with a maximum peak at 44.5%, which may be interpreted as representing the hyaloclastites and basaltic lavas. Histograms with distribution of SiO₂ for each well are given in Appendix III.

SiO₂ (%)

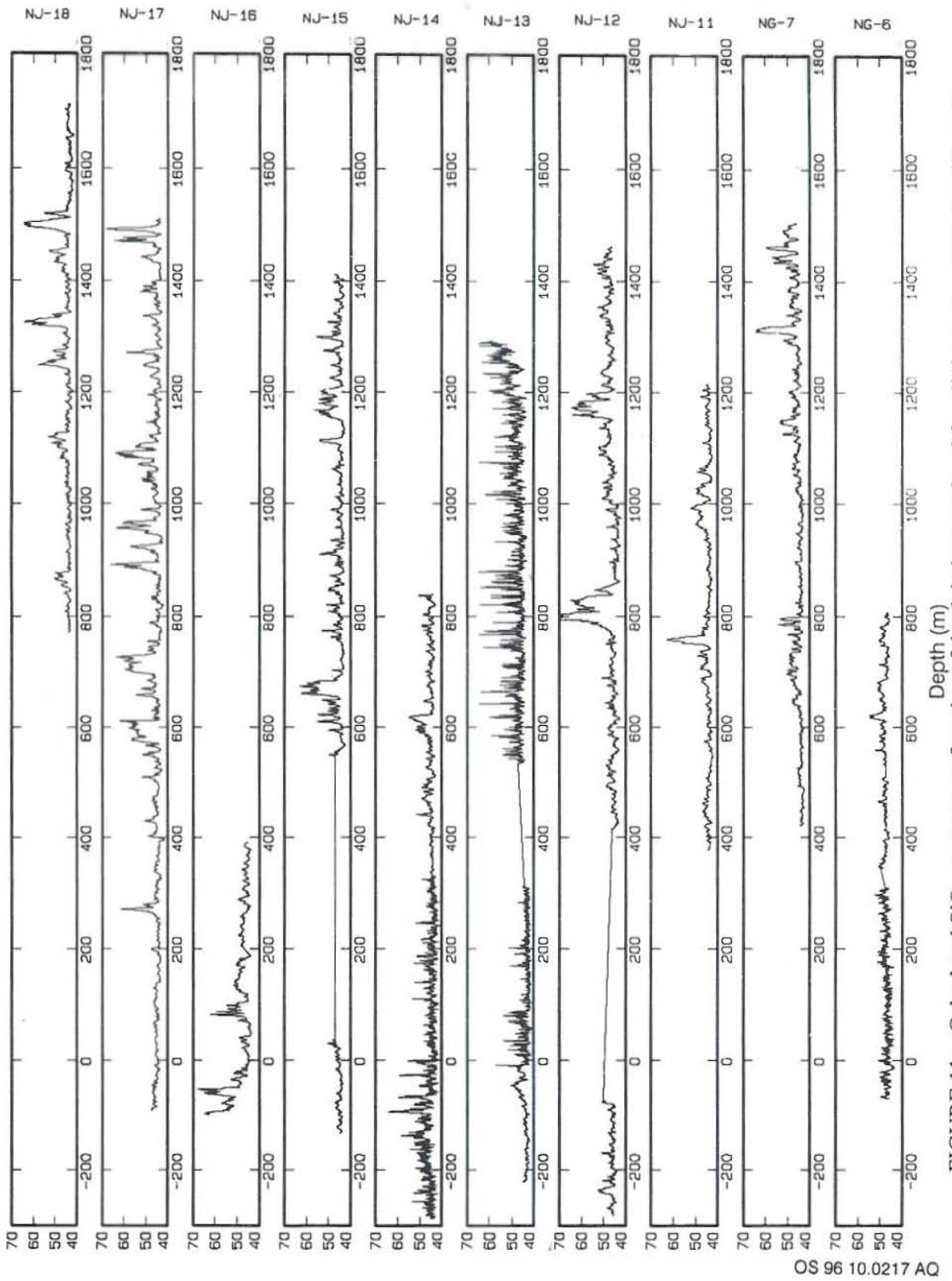


FIGURE 11: Calculated SiO₂ content as a function of depth below sea level for all the analysed Nesjavellir wells

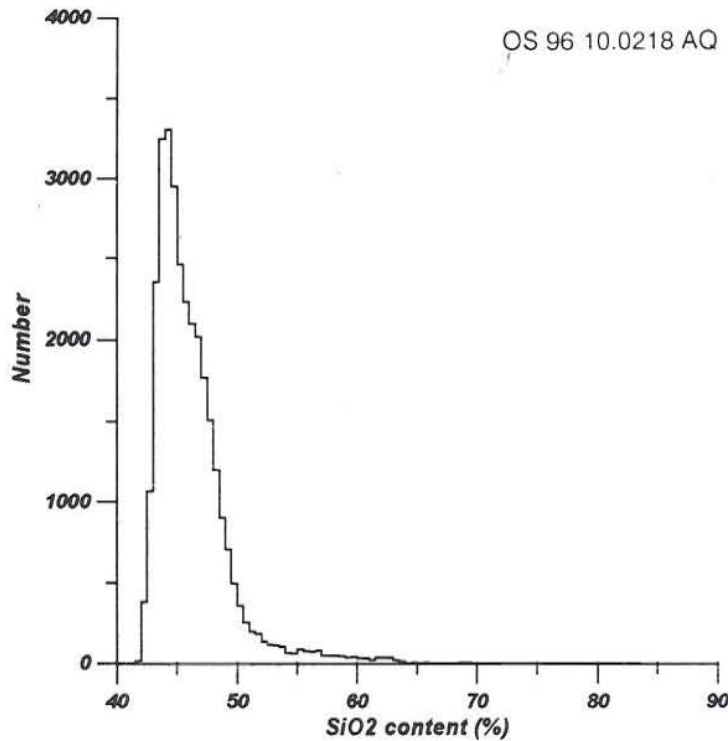


FIGURE 12: Distribution of the combined SiO₂ content of wells NG-6, NG-7, NJ-11, NJ-12, NJ-13, NJ-14, NJ-15, NJ-16, NJ-17 and NJ-18

Wells NG-9 and NG-10 are not included in the present analysis on silica content because natural gamma log data was not available for NG-9 and no good calibration for well NG-10 was detected.

Figure 13 presents the crossplot of SiO₂ content against porosity for well NJ-17. For the other wells the crossplots have a similar behaviour. A major density of dots around 45% of silica content can be observed and the porosity values are distributed in the same proportion both lower and higher than 20%. The explanation for this behaviour is the predominant distribution of hyaloclastites and basaltic lava layers as a function of the depth in the wells. An even more scattered density distribution of values of SiO₂ content higher than 45% and lower than 70%, might be associated with the intermediate and acidic intrusions present in the rock pile. A crossplot of silica content against porosity for each well is presented in Appendix IV.

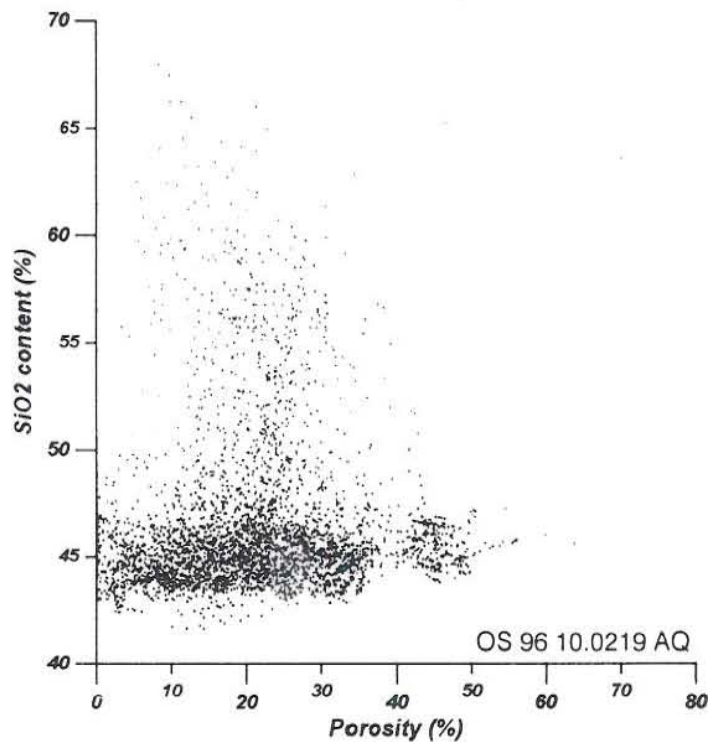


FIGURE 13: A crossplot for silica content vs. porosity for well NJ-17

5. COMPARISON OF GEOPHYSICAL LOGS AND OTHER GEOLOGICAL DATA

The study of porosity distribution is done in two steps. This refers to the geological information. In the upper part, from surface to 400 m below sea level (m b.s.l.), basaltic hyaloclastite formation dominates the rock sequence, whereas the lower part (below 400 m b.s.l.) is characterized by basaltic lava series with sparse interbedded hyaloclastites. Also layers with relatively high resistivity have been found below 400 m b.s.l., which are located under low-resistivity layers (Árnason et al., 1986). The mean porosity has been determined for these two intervals from the surface to 400 m b.s.l. and from 400 to 2000 m b.s.l. for all the wells.

Figure 14 which shows the mean porosity in the upper part indicates lower porosity (less than 24%) in the central part of the well field than in the outer part, while in the lower part (Figure 15) an inverse behaviour is recorded, with mean porosity higher than 24% in the central part of the well field and below that in the outer part. This is explained by the fact that the upper part includes the caprock of the geothermal system, which is self-sealed because of hydrothermal alteration. On the other hand, in both maps the contours are elongated from southwest to northeast, which can be associated with the fracture trend in the field. This elongated shape of the mean-porosity contours is similar to the behaviour of other parameters of the field like pressure and temperature (Gunnarsson et al., 1992). There is a good correlation between zones of relatively high porosity determined from the porosity logs and location of the hyaloclastite layers in the geological cross-sections (Figures 16 and 17).

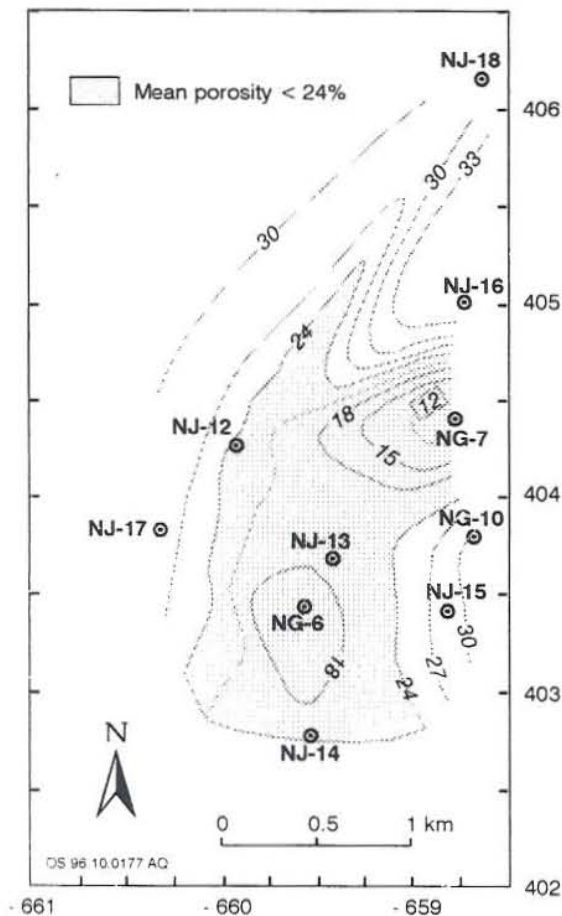


FIGURE 14: Mean porosity contours for the depth interval from surface to 400 m b.s.l.

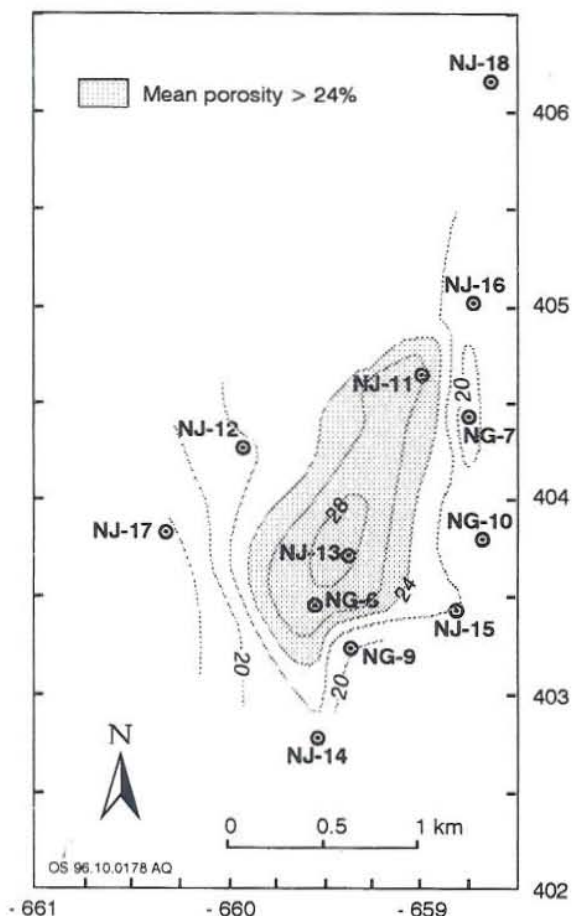


FIGURE 15: Mean porosity contours for the depth interval from 400 to 2000 m b.s.l.

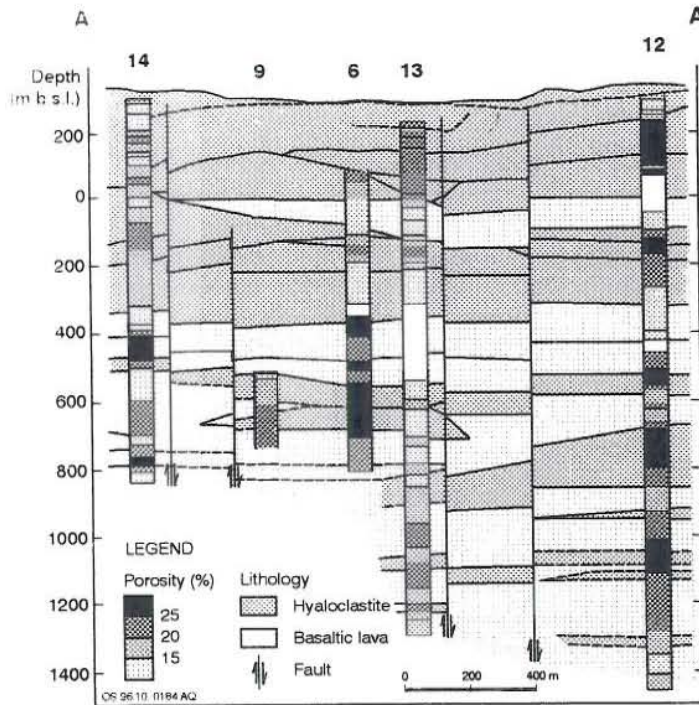


FIGURE 16: Comparison between estimated porosity and geological cross-section AA' (mod. from Franzson, 1988)

The calculated porosity values from the neutron-neutron logs have been compared with the porosity values given in the 1992 numerical model by Bødvarsson (1993) with L and R layer. An average porosity value was calculated for the two depth intervals (600-1000 m and 1000-1800 m) for each well. Since the porosities calculated from the neutron-neutron logs are much higher than the values given in the 1992 model, they were categorised into three groups, low, medium and high porosities. The same was done for the 1992 model (see Table 3). The result for each layer has been summarized in Tables 4 and 5. There it can be seen that for the L-layer the comparison is rather good, but not for the R-layer. Figures 18 and 19 show the calculated average porosities for both layers.

TABLE 3: Categories established to compare the results of porosity logs with the 1992 numerical model from Bødvarsson (1993)

Category	Porosity logs	1992 model
	Porosity (%)	Porosity (%)
Low porosity, L	< 20	1 - 2
Medium porosity, M	20 - 24	3 - 4
High porosity, H	> 24	5 - 10

TABLE 4: Comparison of porosity categories between results of porosity logs and the 1992 numerical model for the depth interval 600-1000 m b.s.l. (L layer)

Well	Porosity logs		1992 model	
	Porosity (%)	Category	Porosity (%)	Category
NG-7	18.3	L	2	L
NJ-13	16.4	L	2	L
NJ-18	20.0	M	2	L
NG-10	23.1	M	3.5	M
NJ-14	21.7	M	3.5	M
NJ-15	23.4	M	3.5	M
NG-6	29.1	H	10	H
NG-9	22.8	M	10	H
NJ-11	27.4	H	5	H
NJ-12	22.5	M	10	H
NJ-16	20.0	M	5	H
NJ-17	20.8	M	5	H

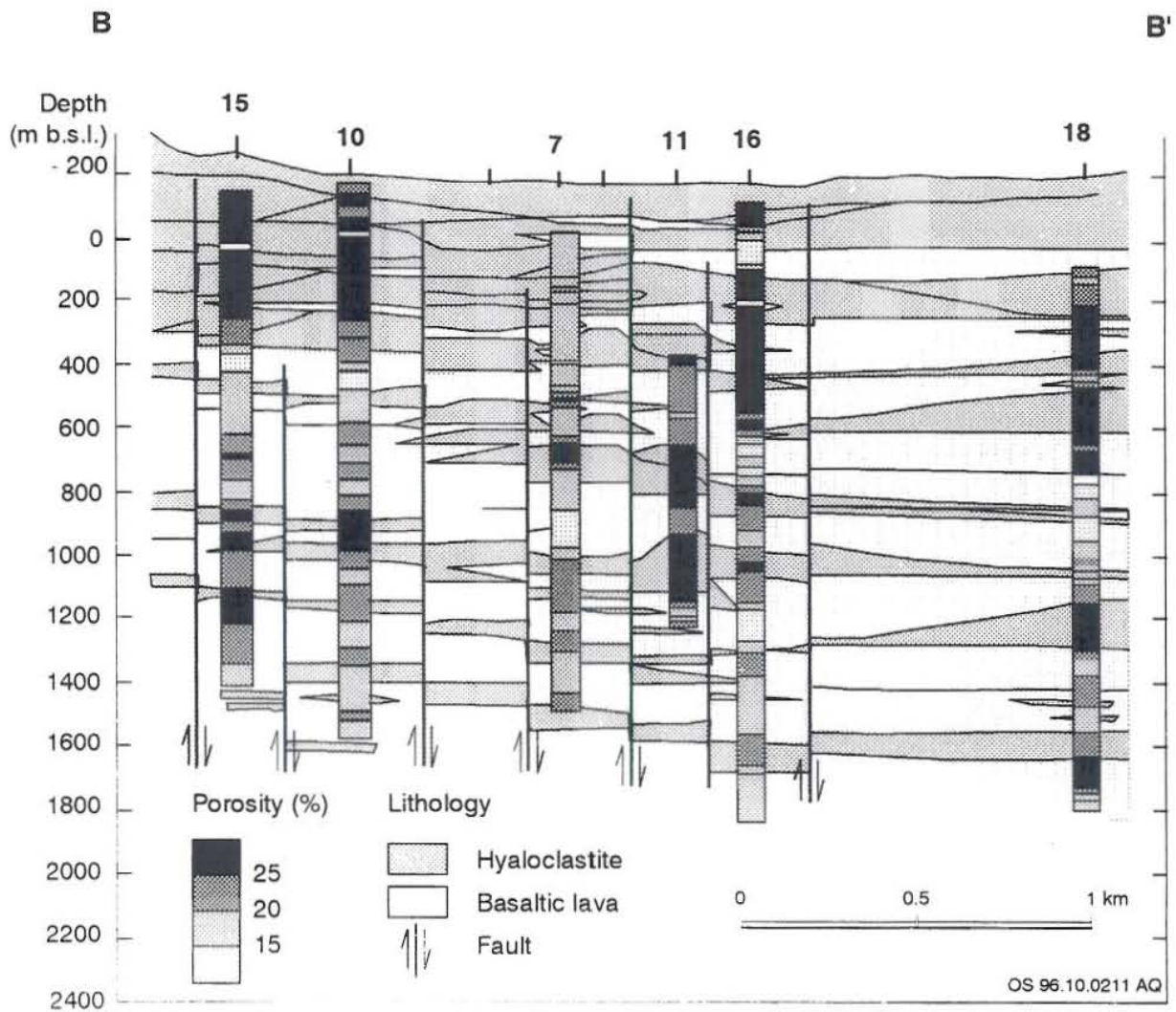


FIGURE 17: Comparison between estimated porosity and geological cross-section BB' (modified from Franzson, 1988)

For the R layer (from 1000 to 1800 m b.s.l.) there is not a very good correlation, mainly because wells NG-10 and NJ-11 have quite different categories. According to the values of porosity from the porosity logs, well NG-10 has relatively low porosity whereas in the model it has relatively high porosity. On the other hand, well NJ-11 has a low porosity according to the model whereas the porosity logs give it a relatively high porosity, as shown in Table 5. Figures 18 and 19 show the low, medium and high mean-porosity zones for the L and R layers, respectively, determined using the porosity log data.

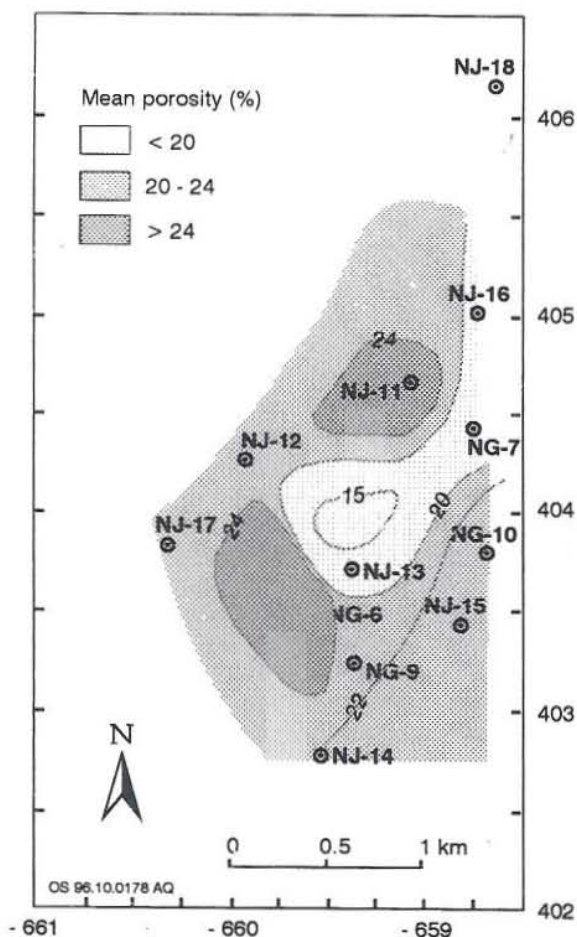


FIGURE 18: Low, medium and high mean-porosity zones for the depth interval 600-1000 m b.s.l., determined using the porosity log data

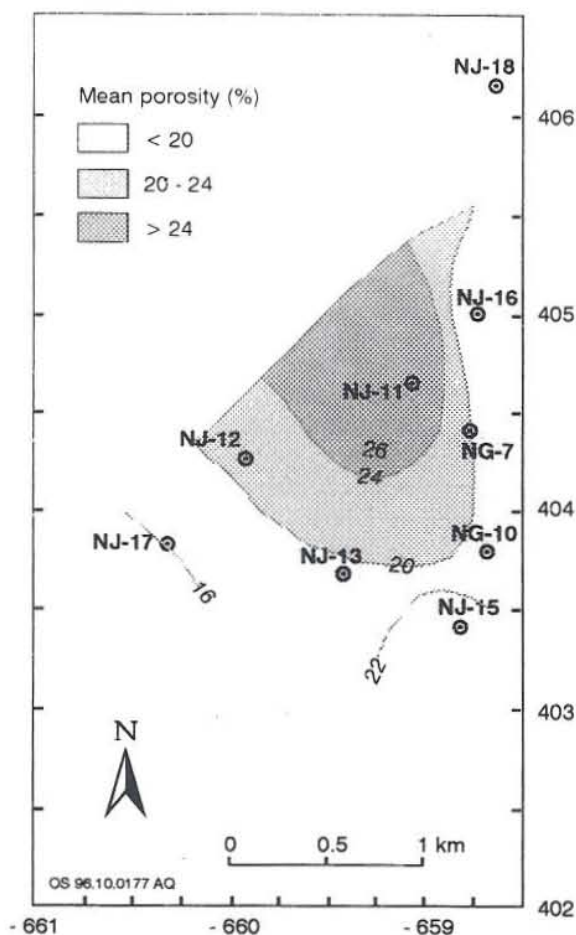


FIGURE 19: Low, medium and high mean-porosity zones for the depth interval 1000-1800 m b.s.l., determined using the porosity log data

TABLE 5: Comparison of porosity categories between results of porosity logs and 1992 numerical model for the depth interval 1000-1800 m b.s.l. (R layer)

Well	Porosity logs		1992 model	
	Porosity (%)	Category	Porosity (%)	Category
NG-7	20.3	M	2	L
NJ-11	28.0	H	1	L
NJ-16	18.2	L	2	L
NJ-18	23.0	M	2	L
NJ-12	21.3	M	3.5	M
NJ-13	18.5	L	3.5	M
NJ-17	16.0	L	3.5	M
NG-10	19.5	L	5	H
NJ-15	23.1	M	5	H

6. CONCLUSIONS

The main conclusions derived from this study are the following:

1. An unimodal distribution has been encountered for the porosity, with a maximum at 19%. Also the distribution of the silica content is unimodal, with a maximum at 44.5%.
2. A good correlation is between relatively high porosity zones and location of hyaloclastite layers.
3. For the depth interval 600-1000 m b.s.l., a good correlation has been found between the porosity categories, determined using the porosity logs data and the porosity categories from the 1992 numerical model of this geothermal field. Even though there is a striking discrepancy in the porosity categories of wells NG-10 and NJ-11, there is also in general a good correlation in the results of the other wells, for the depth interval 1000-1800 m b.s.l. (R layer).
4. The major feedzones in the wells found during drilling are located in relatively high porosity zones determined by means of the neutron-neutron logs.
5. Even though the SiO₂ logs show several peaks which can be associated with intermediate and acidic magmatic intrusions, there is not a clear correlation between the wells.
6. Crossplots of SiO₂ against porosity show a major density of dots around 45% silica content and the porosity values are distributed in the same proportion both lower and higher than 20%, which is explained for the predominant distribution of hyaloclastites and basaltic lavas layers as a function of the depth in the wells.
7. The even more scattered lower density distribution of values of SiO₂ content higher than 45% and lower than 70% in the crossplots, has been associated with the intermediate and acidic intrusions present in the rock pile.
8. In the upper part of the rock sequence the mean porosity in the central part of the well field is lower than the porosity in the outer part, while in the lower part of the rock sequence the mean porosity in the central part of the well field is higher than in the outer part. This is in agreement with the effect of the caprock in the upper part of the geothermal system.
9. The mean porosity contours are elongated from southwest to northeast, which is associated with the fracture trend in the field. This result is similar to the behaviour shown by other parameters of the field like pressure and temperature.

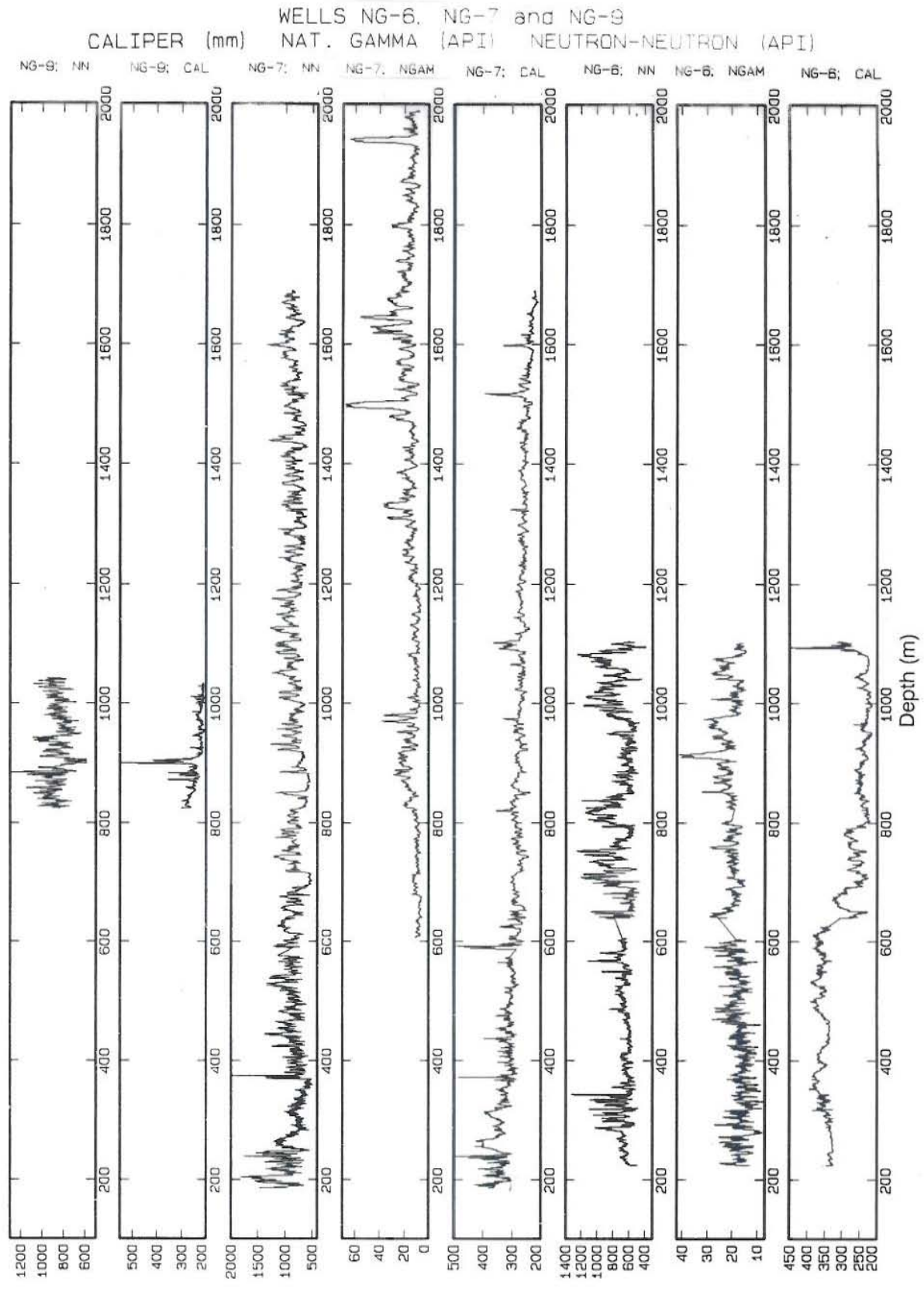
ACKNOWLEDGEMENTS

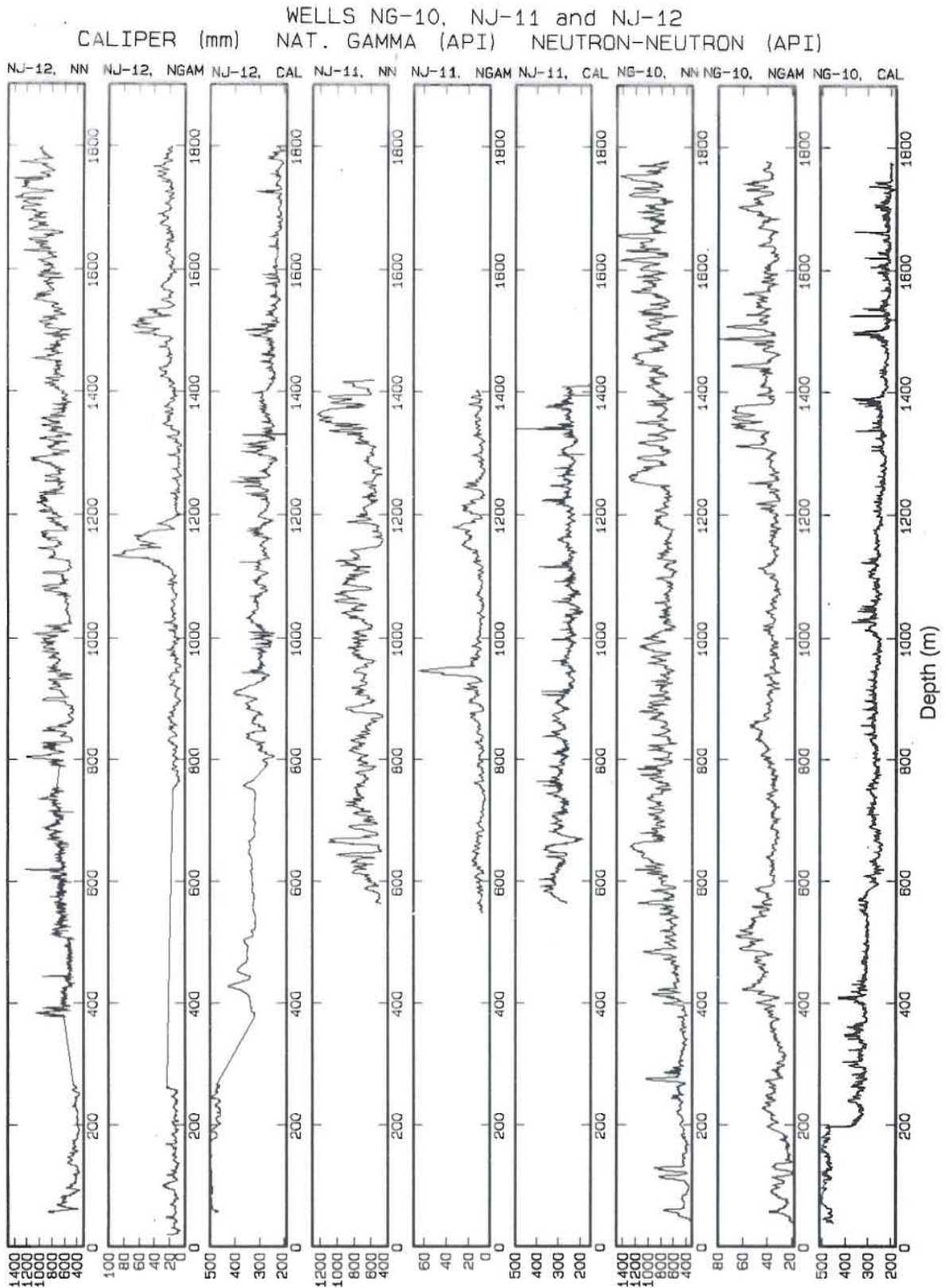
I am very grateful to everyone involved for giving me the opportunity to participate in the UNU Geothermal Training Programme, especially Dr. Ingvar Birgir Fridleifsson, Director of the programme and the management of Comisión Ejecutiva Hidroeléctrica del Río Lempa (C.E.L.), División de Recursos Geotérmicos (GEOCEL) for permission to attend this specialized course. I want to thank Mr. Lúdvík S. Georgsson and Ms. Gudrún Bjarnadóttir for their special help and guidance throughout the training period. I want to express my hearty gratitude to Hilmar Sigvaldason and Thordur Arason, my advisors, for their guidance and for sharing their knowledge and experience. Also thanks to Helga Tulinius and all the lecturers and staff members at Orkustofnun for their teaching and assistance. Deepest thanks to my family, especially to my parents, my wife Angela, my daughter Ana María and my son Allan Arturo for giving me their invaluable spiritual support during all these months of physical separation.

REFERENCES

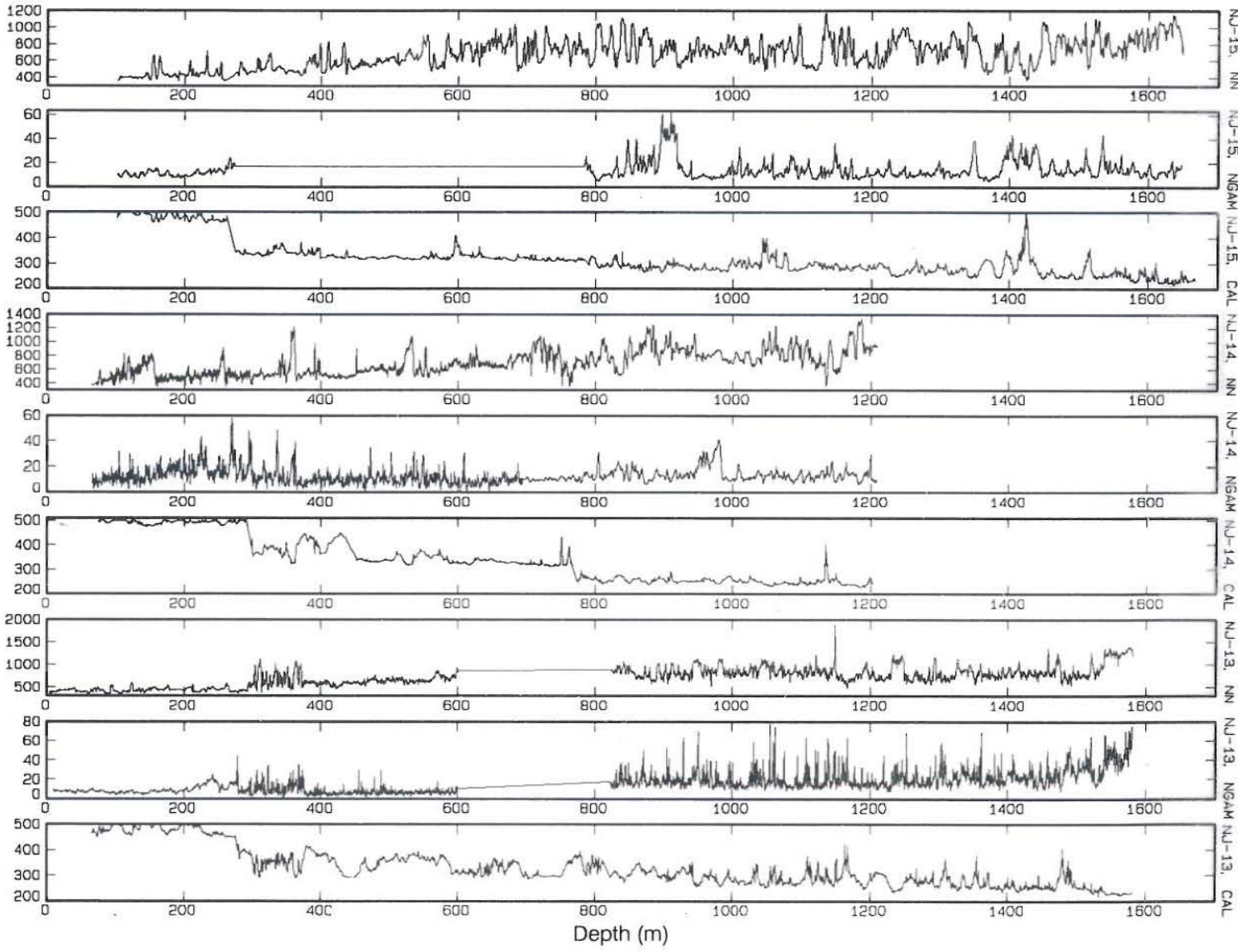
- Arason, P., 1993: *The BHM program*. Orkustofnun, Reykjavík, Iceland.
- Árnason, K., Haraldsson, G.I., Johnsen, G.V., Thorbergsson, G., Hersir, G.P., Saemundsson, K., Georgsson, L.S., and Snorrason, S.P., 1986: *Nesjavellir, geological and geophysical exploration in 1985*. Orkustofnun, Reykjavík, report OS-86014/JHD-02 (in Icelandic), 125 pp.
- Böðvarsson, G.S., 1993: *Recalibration of the three-dimensional model of the Nesjavellir geothermal field*. Report prepared for the Reykjavík District Heating, Iceland, viii + 111 pp.
- Böðvarsson, G.S., Björnsson, S., Gunnarsson, Á., Gunnlaugsson, E., Sigurdsson, Ó., Stefánsson V., and Steingrímsson, B., 1990: The Nesjavellir geothermal field, Iceland. Part 1. Field characteristics and development of a three-dimensional numerical model. *J. Geotherm. Sci. and Tech.*, 2-3, 189-228.
- Chambre Syndicale de la Recherche et de la Production du Pétrole et du Gaz Naturel, 1984: *Wireline Logging Tool Catalog*. Editions Technip, Paris, xi + 169 pp.
- Franzson, H., 1988: *Nesjavellir - Borehole geology and permeability in the reservoir*. Orkustofnun, Reykjavík, report OS-88046/JHD-09 (in Icelandic), 58 pp.
- Franzson, H., Gudmundsson, Á., Fridleifsson, G.Ó. and Tómasson, J., 1986: Nesjavellir high-temperature field, SW-Iceland - reservoir geology. *Extended abstracts of 5th International Symposium on Water-Rock Interaction, Reykjavík, 1986*, 210-213.
- Franzson, H. and Sigvaldason, H., 1985: *Nesjavellir well NG-8, geology, alteration, logging and aquifers*. Orkustofnun, Reykjavík, report OS-85120/JHD-16 (in Icelandic), 33 pp.
- Gunnarsson, Á., Steingrímsson, B.S., Gunnlaugsson, E., Magnússon, J., and Maack, R., 1992: Nesjavellir geothermal co-generation power plant. *Geothermics*, 21-4, 559-583.
- Hearst, J.R., and Nelson, P.H., 1985: *Well logging for physical properties*. McGraw-Hill Book Company, New York, xv + 571 pp.
- Helander, D.P., 1983: *Fundamentals of formation evaluation*. Oil and Gas Consultants International (OGCI) Publications, Tulsa, Oklahoma. xi + 332 pp.
- Keys, W.S., and McCary, L.M., 1971: Application of borehole geophysics to water-resources investigation. In: *Techniques of water-resources investigations*. Geological Survey, Book 2-E, Washington, USA, 126 pp.
- Serra, O., 1984: *Fundamentals of well-log interpretation; Vol. 1. The acquisition of logging data*. Development in Petroleum Science 15A, Elsevier Science Publishers, Amsterdam, xii + 423 pp.
- Stefánsson, V., Gudmundsson, Á., and Emmerman, R., 1982: Gamma ray activity in Icelandic rocks. *The Log Analyst*, XXIII-6, 11-16.
- Stefánsson, V., and Steingrímsson, B., 1980: *Geothermal logging I, an introduction to techniques and interpretation*. Orkustofnun, Reykjavík, report OS-80017/JHD-09, 117 pp.
- Steingrímsson, B., Gudmundsson, Á., Franzson, H., and Gunnlaugsson, E., 1990: Evidence of a supercritical fluid at depth in the Nesjavellir field. *Proceedings of the 15th Workshop on Geothermal Reservoir Engineering, Stanford University, California*, 81-88.

APPENDIX I: Caliper, natural gamma and neutron-neutron logs in the Nesjavellir wells

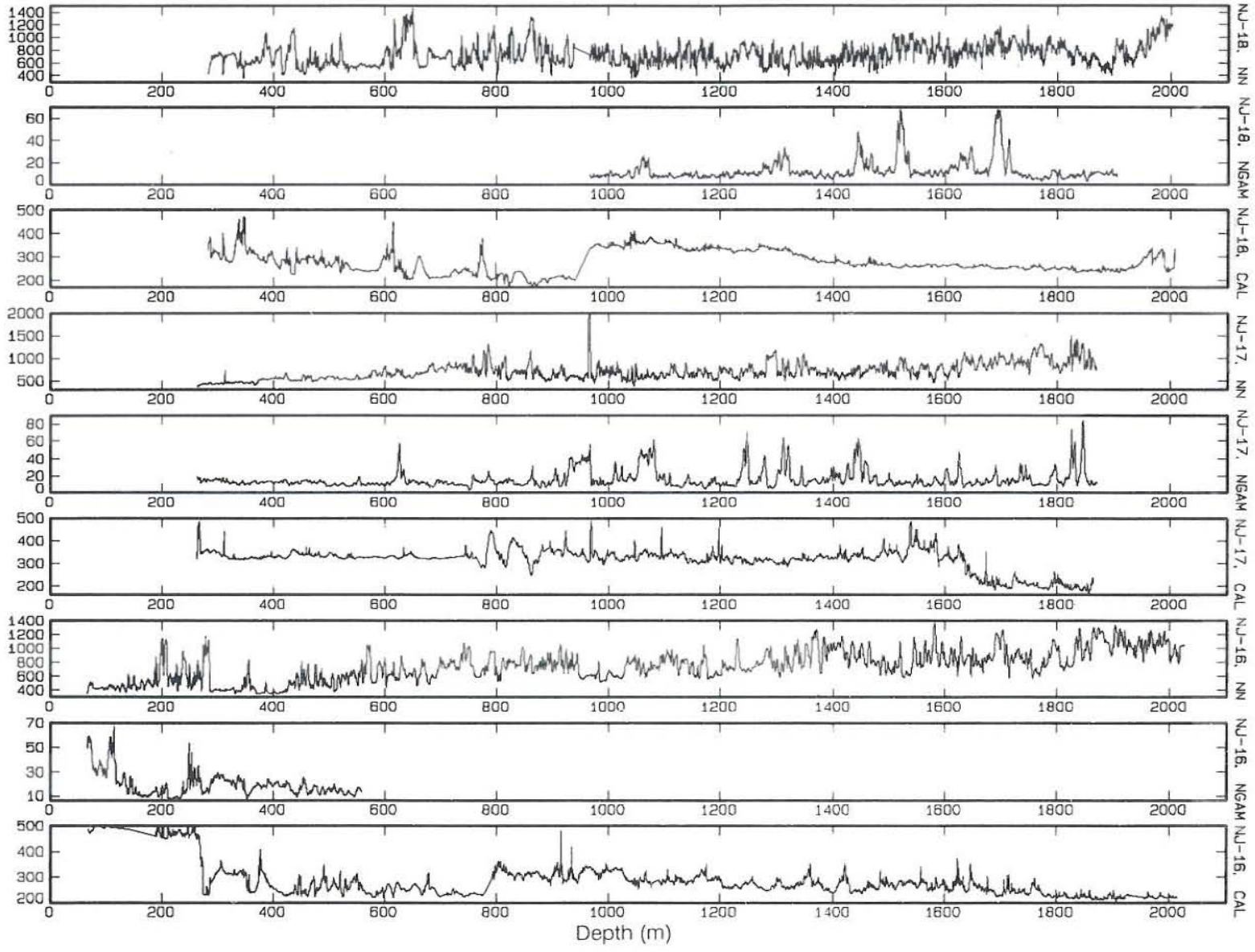




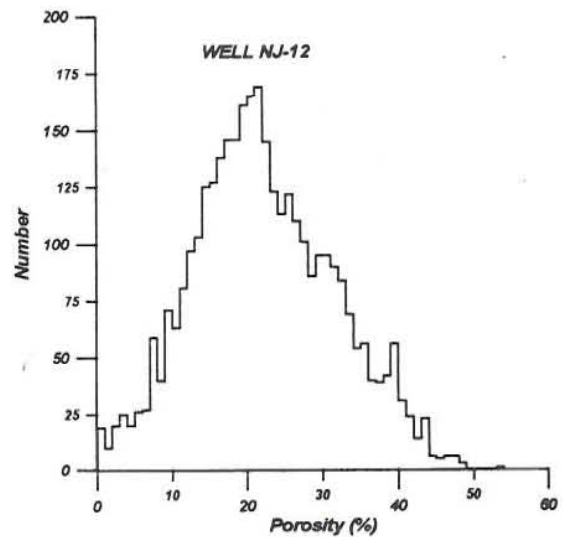
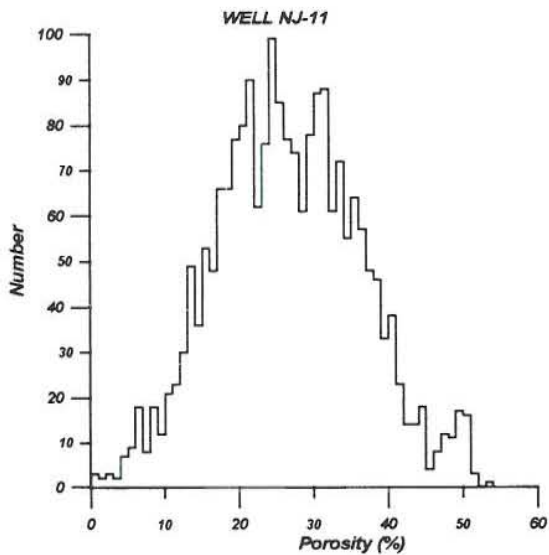
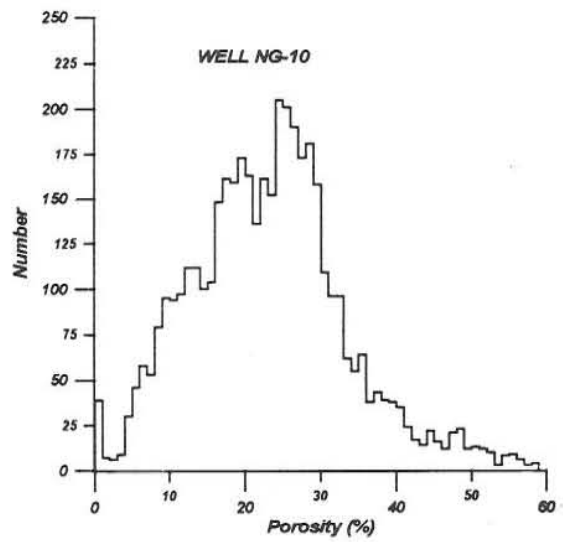
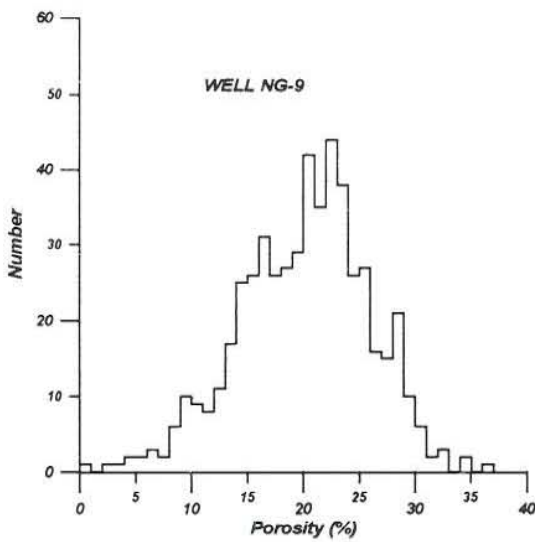
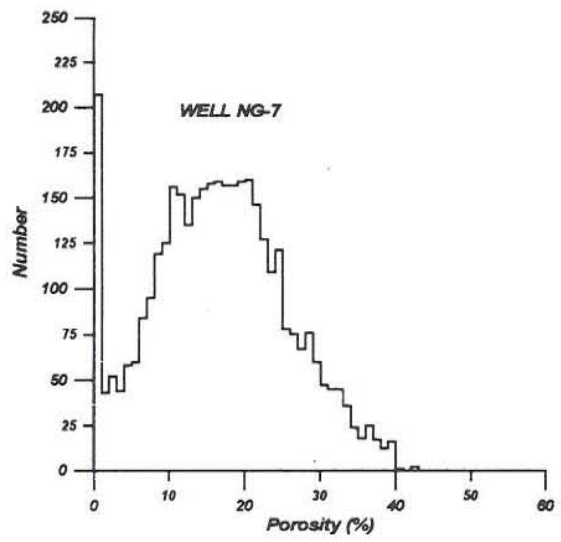
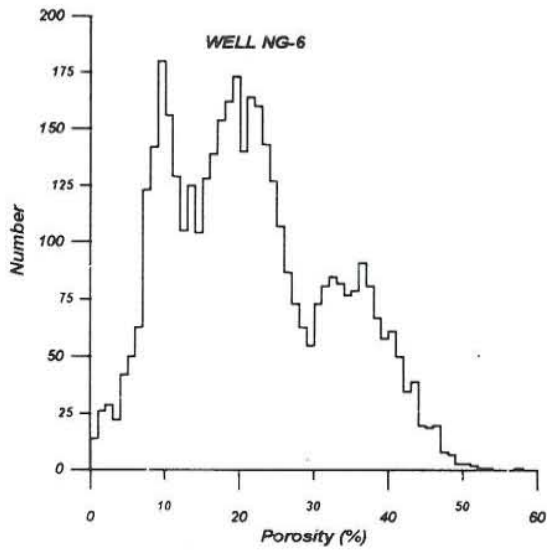
WELLS NU-13, NU-14 and NU-15
CALIPER (mm) NAT. GAMMA (API) NEUTRON-NEUTRON (API)

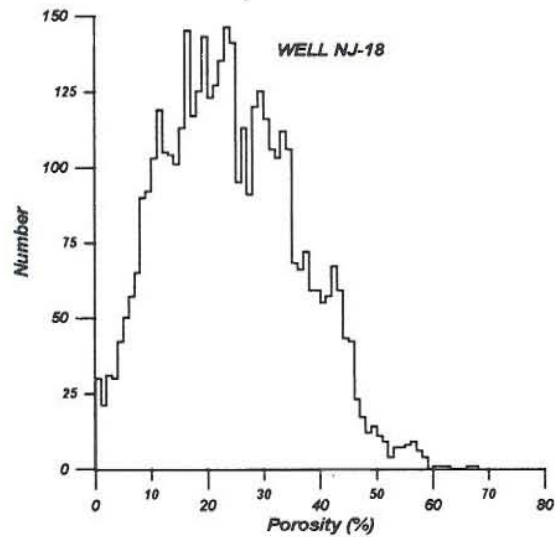
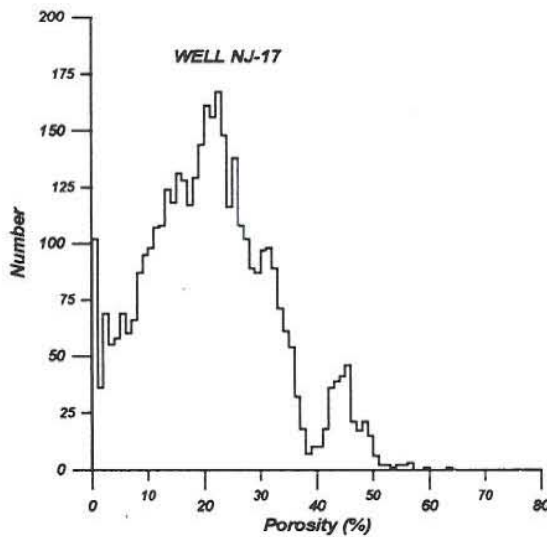
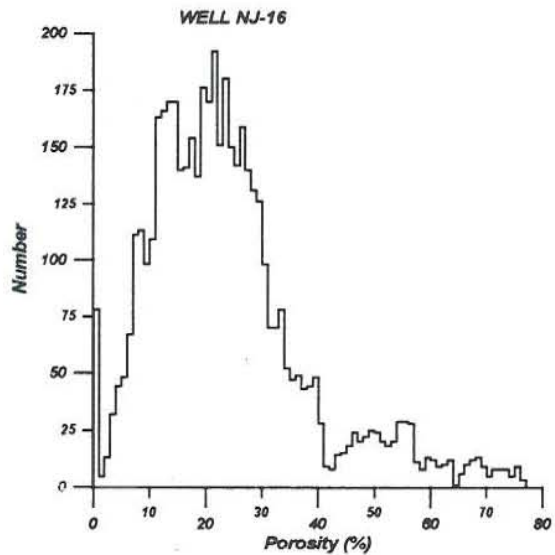
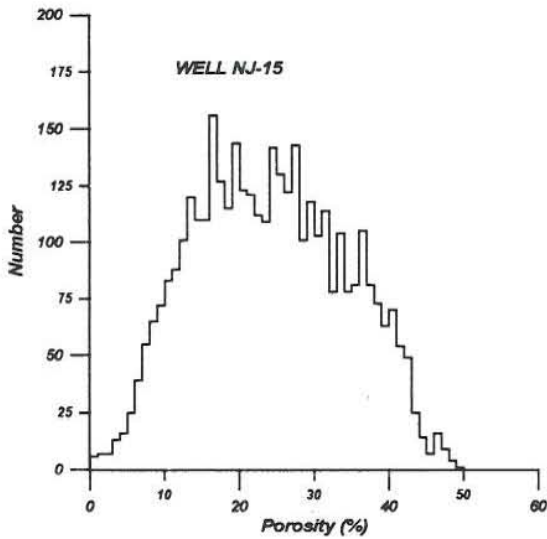
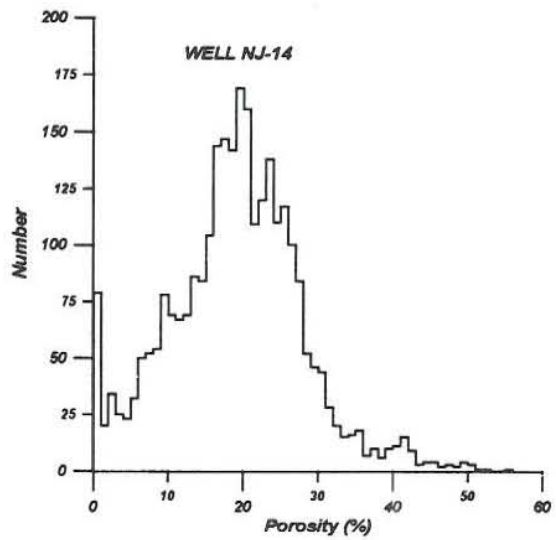
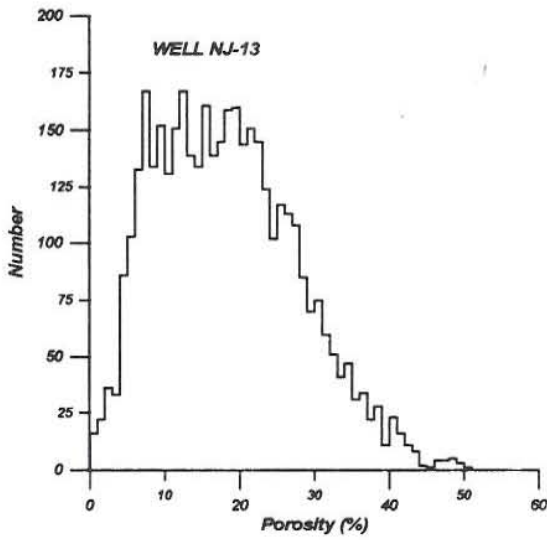


WELLS NU-16, NU-17 and NU-18
CALIPER (mm) NAT. GAMMA (API) NEUTRON-NEUTRON (API)

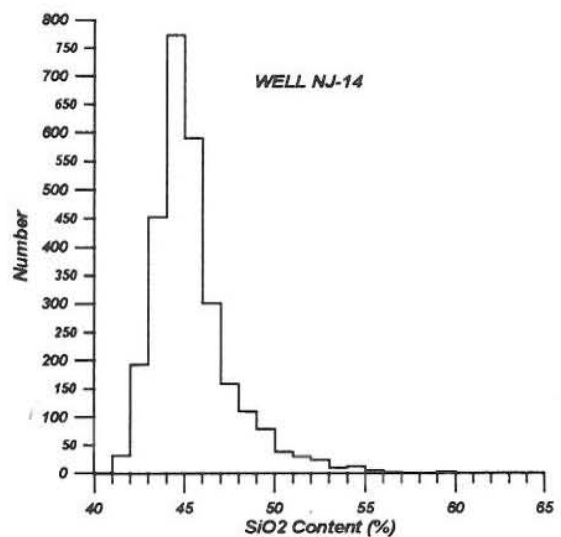
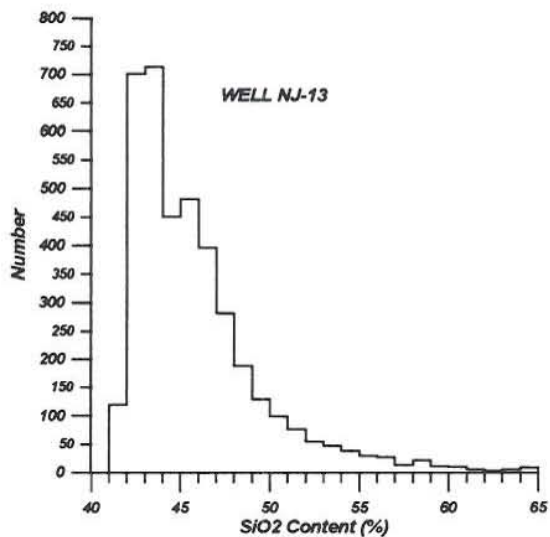
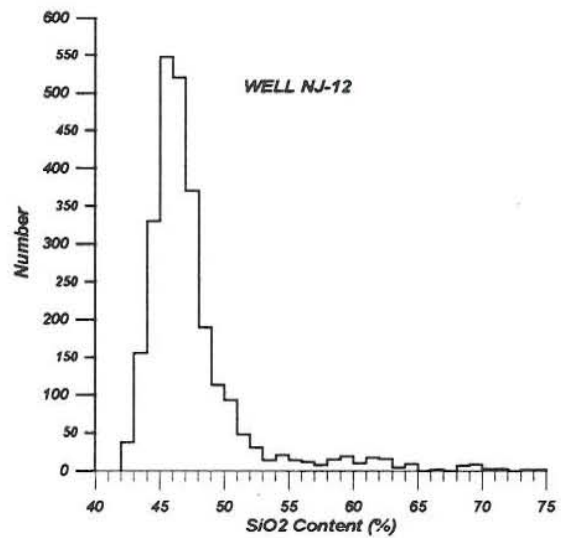
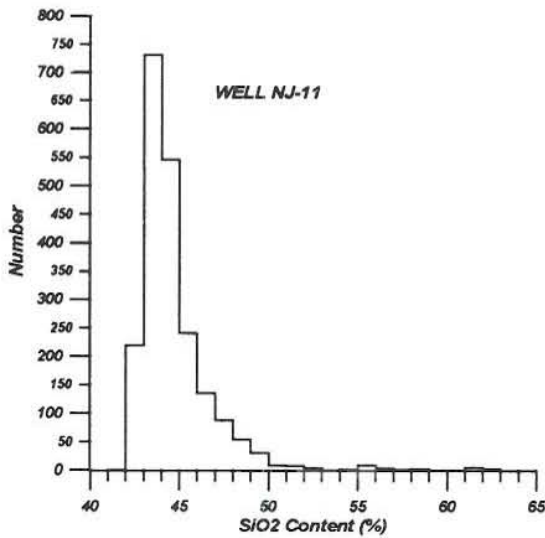
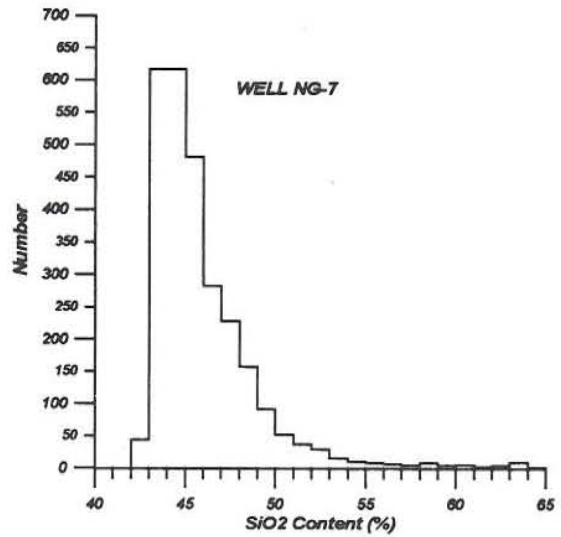
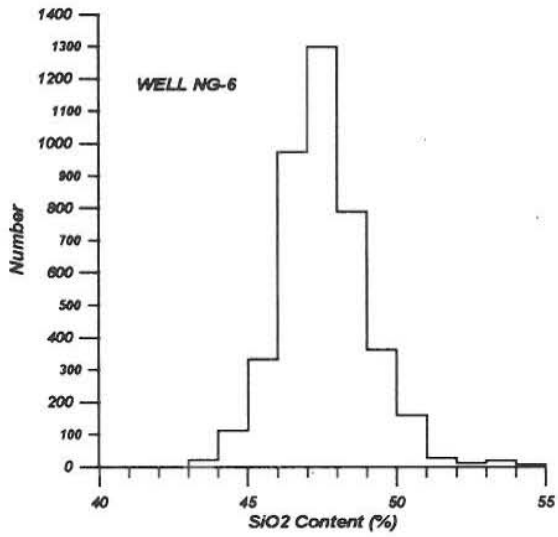


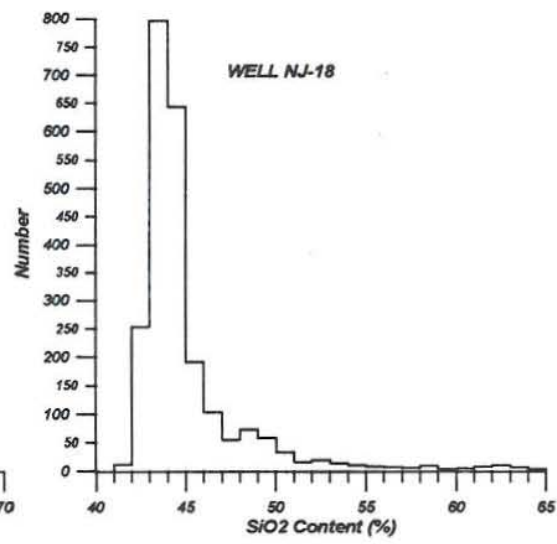
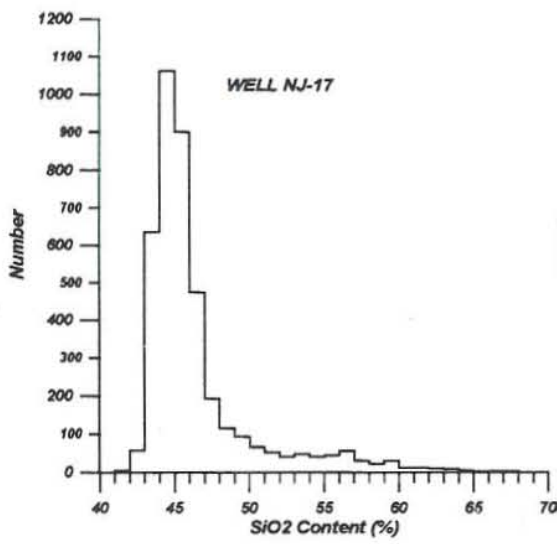
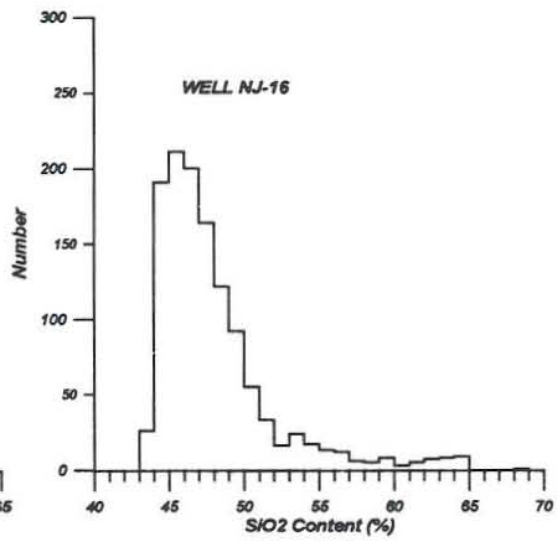
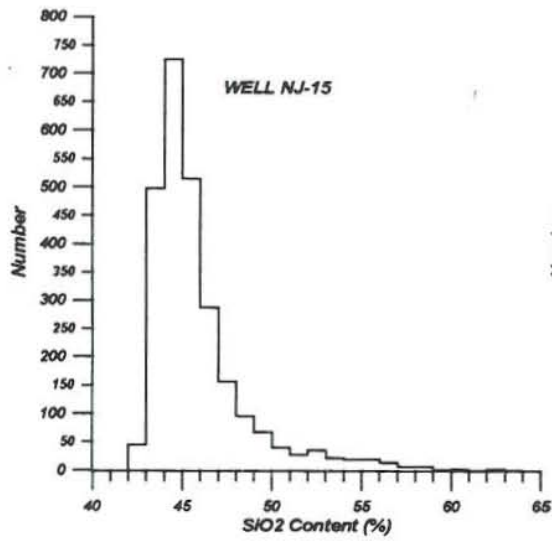
APPENDIX II: Porosity distribution histograms for the Nesjavellir wells





APPENDIX III: SiO₂ content distribution histograms for the Nesjavellir wells





APPENDIX IV: SiO₂ content against porosity crossplots for the Nesjavellir wells

